Structural evolution and the partitioning of deformation during basin growth and inversion: a case study from the Mizen Basin Celtic Sea, offshore Ireland

P. Rodríguez-Salgado[1, 2], C. Childs[1,2], P.M. Shannon[1,3] & JJ. Walsh[1,2]

[1] Irish Centre for Research in Applied Geosciences (iCRAG), University College Dublin, Belfield, Ireland (pablo.rodriguez-salgado@icrag-centre.org)

[2] Fault Analysis Group, School of Earth Sciences, University College Dublin, Belfield, Ireland

[3] Marine and Petroleum Geology Research Group, School of Earth Sciences, University College Dublin, Belfield, Ireland

Abstract

The Celtic Sea basins lie on the continental shelf between Ireland and northwest France and consist of a series of ENE - WSW trending elongate basins that extend from St George's Channel Basin in the east to the Fastnet Basin in the west. The basins, which contain Triassic to Neogene stratigraphic sequences, evolved through a complex geological history that includes multiple Mesozoic rift stages and later Cenozoic inversion. The Mizen Basin represents the NW termination of the Celtic Sea basins and consists of two NE-SW trending half-grabens developed as a result of the reactivation of Caledonian and Variscan faults.

The faults bounding the Mizen Basin were active as normal faults from Early Triassic to Late Cretaceous times. Most of the fault displacement took place during Berriasian to Hauterivian (Early Cretaceous) times, with a NW-SE direction of extension. A later phase of Aptian to Cenomanian (Early to Late Cretaceous) N-S oriented extension gave rise to E-W-striking minor normal faults and reactivation of the pre-existing basin-bounding faults that propagated upwards as left-stepping arrays of segmented normal faults. In common with most of the Celtic Sea basins, the Mizen Basin experienced a period of major erosion, attributed to tectonic uplift, during the Paleocene. Approximately N-S Alpine regional

compression causing basin inversion is dated as Middle Eocene to Miocene by a well preserved syn-inversion stratigraphy. Reverse reactivation of the basin bounding faults was broadly synchronous with the formation of a set of near-orthogonal NW-SE dextral strike-slip faults so that compression was partitioned onto two fault sets the geometrical configuration of which is partly inherited from Palaeozoic basement structure.

The segmented character of the fault forming the southern boundary of the Mizen Basin was preserved during Alpine inversion so that Cenozoic reverse displacement distribution on syn-inversion horizons mirrors the earlier extensional displacements. Segmentation of normal faults therefore controls the geometry and location of inversion structures, including inversion anticlines and the back rotation of earlier relay ramps.

Keywords

Strike-slip, basin inversion, fault segmentation, Cenozoic inversion, inversion structures

1. Introduction

Basin inversion is defined as the uplift of an extensional basin as a result of crustal shortening by tectonic compression or transpression (Glennie & Boegner, 1981; Bally, 1984; Harding, 1985; Williams *et al.*, 1989; Buchanan & Buchanan, 1995; Turner & Williams, 2004; Bonini *et al.*, 2012). During basin inversion, shortening frequently takes place both through reactivation of pre-existing faults and the formation of a wide range of compressional structures such as reverse faults, folds and strike-slip faults (Coward, 1983; Bally, 1984; Turner & Williams, 2004). The size, style and distribution of inversion structures is dependent on the different inversion mechanisms which in turn, are controlled by basement structural fabric, pre-inversion normal fault geometry, mechanical strength and anisotropy of the basin fill (Turner & Williams, 2004), and the magnitude of shortening (Tesón *et al.*,

2013). Recent work suggests that the the particular faults within a system of normal faults that are inverted is also partly determined by pre-existing fault size, with the largest faults, in terms of displacement and length, preferentially reactivated, , and with the distribution of reverse displacement on inverted faults sometimes being similar to that on the pre-existing normal fault (Reilly et al. 2017).. In this paper we examine in detail the geometry and displacement distribution on a basin-bounding segmented normal fault array and its relationship to the reverse displacement distribution when it is reactivated in compression.

Partitioning of displacement onto structures of different orientation and faulting mode is a common feature of zones of transpressional and transtensional strain where oblique movements are accommodated by strike-slip faulting in combination with purely contractional or extensional structures (Tikoff & Teyssier, 1994; Dewey et al. 1998). The likelihood of strain partitioning is enhanced in the presence of a reactivated pre-existing structural grain (Jones and Tanner, 1995) which can lead to increased structural complexity, including compressional structures in extension-dominated settings (De Paola et al. 2005), so that structures that resemble inversion features result from oblique opening. The fault systems of the Mizen Basin provide an example of partitioning of displacement onto compressional and strike-slip faults without a strong large scale wrench component but under the influence of pre-existing basement structures.

The rift basins and passive margins of the North Atlantic domain of Western Europe experienced regional uplift (Stuevold & Eldholm, 1996; Doré *et al.*, 2002; Praeg *et al.*, 2005; Anell *et al.*, 2009) and tectonic inversion (Riis *et al.*, 1986; Roberts, 1989; Ziegler, 1990b; Gabrielsen *et al.*, 1993; Doré & Lundin, 1996; Vågnes *et al.*, 1998) during the Cenozoic. On the continental shelf of southern Ireland – western UK, where the Mizen Basin is located, a broad regional uplift took place during the Palaeocene-Eocene as evidenced by the absence of preserved Palaeogene and Early Eocene stratigraphy throughout the area. This uplift was

followed by Alpine basin inversion which took place from Middle Eocene to Miocene. This later episode triggered the development of inversion structures controlled by reverse reactivation of rift-related faults, folding and strike-slip faulting.

Several previous studies have focused on understanding the timing and magnitudes of the Cenozoic uplift and the inversion in the Celtic Sea basins (Menpes & Hillis, 1995; Murdoch *et al.*, 1995). Although a large part of the total estimated basin exhumation is attributed to regional uplift (Murdoch *et al.*, 1995), it has not been hitherto possible to isolate the individual effects of each episode or to investigate details of the timing and growth of the basin inversion structures. This is mainly due to an incomplete and poorly preserved syn-inversion stratigraphy over most of the Celtic Sea basins; in the central parts of the North and South Celtic Sea basins Upper Cretaceous chalk strata are at the sea-bed (Fig. 1a). Uplift and erosion were most pronounced in the central part of the North Celtic Sea Basin, becoming more subdued towards the west, particularly in the Fastnet and Mizen basins, where a relatively complete sequence of Middle Eocene to Pliocene has been preserved. Analysis of the Mizen Basin therefore provides an opportunity to gain insights into the style and timing of inversion structures in the wider Celtic Sea area.

The Mizen Basin represents the western termination of the Celtic Sea basins (Fig. 1) and consists of two NE-SW trending half-grabens, bounded by northward-dipping faults developed as a result of the reactivation of both Caledonian and Variscan faults (McCann & Shannon, 1993). The basin is the SW extension of the North Celtic Sea Basin (NCSB) and is separated from the Fastnet Basin to the south by the Fastnet Spur a NE plunging basement ridge (Craven, 1995), Fig. 1. Early research on the Mizen Basin, initially interpreted as a segment of the North Celtic Sea Basin, was carried out by McCann and Shannon (1993) who described the basin's structural configuration and the Early Cretaceous stratigraphy. Subsequent work described the structure of the pre-Mesozoic basement and the influence of

Variscan and Caledonian lineaments on the later basin development (McCann & Shannon, 1994). Craven (1995) used the term Mizen Basin for first time, and briefly described the source rock potential of the basin.

To date, published studies of the Mizen Basin and surrounding areas have been based on relatively sparse 2-D seismic reflection data. The present work is based on a 3-D seismic reflection survey combined with wireline log and biostratigraphic data (Fig. 2). The extensive 3-D seismic coverage and well-preserved syn-tectonic stratigraphic sequence makes this an excellent area to study and understand the timing and style of inversion of the Celtic Sea basins that is not possible further to the east. The main aims of this work are to i) document the tectonostratigraphic evolution of the Mizen Basin, ii) highlight the role of non-coaxial extension and shortening on fault reactivation and segmentation and iii) document the style and timing of growth of the Cenozoic inversion structures which are widely distributed along the Atlantic passive margins and are an important target for hydrocarbon exploration.

2. Regional geological development

The evolution of the Celtic Sea basins was strongly influenced by deep-seated crustal lineaments formed during the Palaeozoic as a result of the Caledonian and Variscan orogenic cycles (BIRPS & ECORS, 1986; Cheadle *et al.*, 1987; McGeary *et al.*, 1987; Pinet *et al.*, 1987). The basement structural fabric in Ireland is aligned with the Iapetus suture zone arising from the collision between the Eurasian and North American plates during the late Silurian Caledonian orogeny. This fabric changes from a NE-SW trend in the Leinster massif onshore SE Ireland to a more ENE-WSW trend towards the SW and immediately to the north of the Celtic Sea basins (Gardiner, 1970; Shannon, 1979; Gardiner & Sheridan, 1981).

The Variscan Orogeny, during latest Carboniferous-earliest Permian times, superimposed a pronounced E-W oriented structural fabric on the pre-existing Caledonian fabric. The Variscan lineaments in Ireland were dominantly located in the south along the Variscan Front, which is obliquely intersected by the Celtic Sea basins (Ziegler, 1987). The Variscan structural imprint can be recognised on the rocks outcropping onshore southern Ireland (Gill, 1962; Naylor, 1978; Hitzman, 1999) whereas offshore, these structures are expressed as continuous dipping reflectors beneath the sedimentary basins. These reflectors are regionally interpreted as southward-dipping thrusts (Cheadle *et al.*, 1987; Sibuet *et al.*, 1990; Shannon, 1991) and locally, as northward-dipping backthrusts (McCann & Shannon, 1994). In addition, previous authors (Robinson *et al.*, 1981; Petrie *et al.*, 1989; Tappin, 1994) have reported a series of Variscan NW-SE oriented transfer zones which were later reactivated as strike-slip faults during the Mesozoic rifting and Cenozoic inversion stages.

Rift initiation in the Celtic Sea basins commenced in early Triassic times with the development of small isolated basins (Shannon, 1991; Štolfová & Shannon, 2009). Early syn-rift related deposits were restricted to topographic and fault-bounded depocentres, (Naylor & Shannon, 2011) and are represented by fluvial and aeolian deposits of the Sherwood Sandstone Group. These facies rest unconformably on Devonian strata, with Carboniferous rocks only locally preserved (Barr *et al.*, 1981; Shannon, 1991). During Middle and Upper Triassic times sedimentation became regionally extensive as recorded by the deposition of the Mercia Mudstone Group and the Rhaetian Penarth Limestones Group, representing a basin evolution from transitional to fully marine conditions.

The marine transgressive conditions established during the latest Triassic persisted during early Jurassic times with the deposition of the shallow shelf Lower Sinemurian limestones (Liassic Limestones; Robinson *et al.* (1981). A regressive phase was recorded during the Upper Sinemurian to Pliensbachian with deltaic sandstones prograding towards the east

(Robinson *et al.*, 1981). In mid to late Jurassic times sedimentation in the Celtic Sea basins was restricted to the central parts of the basins whereas the margins were affected by a regionally-developed unconformity (Naylor & Shannon, 1982; Ziegler, 1990a). This period also coincided with localised igneous activity in the western part of the Celtic Sea basins which led to basic intrusive rock emplacement during Bajocian times (Caston *et al.*, 1981). In this area an incomplete Jurassic section that comprises only Liassic shales, is consistent with doming related to igneous intrusions, (Fig. 3) that could have enhanced the magnitude of the uplift and erosion.

Erosion of topography formed during the late Cimmerian tectonic phase combined with low sea levels between latest Jurassic and earliest Cretaceous to provide a widespread unconformity at the base Cretaceous (Figs 1b,c and 3). In the Celtic Sea basins, the late Cimmerian unconformity is best developed on the basin margins and becomes paraconformable in the basin depocentres. Cretaceous sedimentation started in Berriasian times with brackish to fresh water sedimentation often represented by the Purbeck Group (Caston, 1995). Continental fluvial to deltaic and transitional environments continued throughout the lower Cretaceous represented by the Wealden Group following a deepening upwards trend. During Albian times, shallow marine conditions were finally established in the area, represented by the transgressive glauconitic sands of the Greensand Fm., deposited over the Wealden Fm. through a slight unconformity (Taber *et al.*, 1995). Progressively deepening marine conditions continued throughout the Upper Cretaceous marked by the widespread deposition of the Chalk Group from Late Cenomanian to Maastrichtian times (Colin *et al.*, 1981; Murdoch *et al.*, 1995), coinciding with the onset of post-rift thermal subsidence.

During the Cenozoic, the Celtic Sea basins were influenced by both the tectonic inversion associated with the Alpine (Pyrenean) orogeny and by thermal and tectonic events related to

the Atlantic domain. These events led to a marked unconformity at the base Cenozoic (Base Cenozoic unconformity) overlain to the west end of the basin margin by a series of syn-inversion related sequences, bounded by minor unconformities from Middle Eocene to Late Miocene in age (Figs 1b,c and 3).

The Mizen Basin comprises two southward dipping half-grabens bounded by northward-dipping faults (Fig.1c). Both faults have been inverted and show a characteristic cross-sectional geometry with extensional offsets at depth passing upwards, across a null-point to reverse offsets in the syn-inversion sequence and the upper parts of the syn-rift section (Figs 1 and 2). Inversion of the upper parts of the sequence is often seen as a southward-dipping monocline rather than as a discrete fault. The southernmost of the two basin-bounding faults (FS-A) forms the northern edge of the eastward plunging Fastnet High so that the syn-rift section onlaps the Fastnet Spur in its footwall (Fig. 1c).

3. Dataset and methods

The database available for this work comprises a Kirchoff pre-stack time-migrated, three-dimensional reflection seismic survey covering an area of 1570.62 km^2, (CGG Veritas 13MZ3D). The survey has an inline/crossline spacing of 25 and 12.5 m respectively and extends down to a maximum depth of 6 seconds two-way-time (TWT). The seismic survey is presented with reverse polarity (SEG convention) with troughs (red colour) representing a downward increase in acoustic impedance and peaks (blue colour) representing a downward decrease in acoustic impedance. All data extracted from this volume (horizon and isochron maps) are presented in milliseconds two-way-time (ms TWT). The dominant frequency in the studied interval is 30 Hz with an average velocity of 3600 m/s implying a vertical resolution of ca 30 m and an average TWT-metre conversion factor of 1.8m to 1ms TWT: a factor which is used to provide estimates of the metric equivalent of TWT depth and throw values.

The 3D seismic data has been tied to the only well drilled in the Mizen Basin (well 56/12-1) (Fig. 3). In addition, a total of 32 two-dimensional seismic lines from the surveys NCS1983, IR94 and EE-1972 have been tied to eight exploration wells drilled in the Mizen, Fastnet and North Celtic Sea basins (Figs 2 and 3). The wells were tied to the seismic using a synthetic seismogram (Fig. 4). The different syn-rift and syn-inversion related units have been constrained by biostratigraphic data provided in well reports.

A total of eight TWT horizon maps representing pre-, syn- and post-rift and syn-inversion sequences (Figs 5, 6 and 7) and six isochron maps have been generated. The only well drilled in the Mizen Basin was drilled on the crest of an inversion structure and it crosses a limited stratigraphic interval (Fig. 5). As a result, there is no well constraint on the pre-Cretaceous stratigraphic interval in the Mizen Basin and it has been interpreted on the basis of seismic facies correlated on 2D seismic lines to wells in adjacent basins. The first two syn-inversion units (Eocene and Paleocene) were not present at the 56/12-1well location. However, these units are continuous throughout most of the study area and are readily constrained by correlating 2D seismic lines that intersect nearby wells in Fastnet and North Celtic Sea basins with the 3D seismic survey in the Mizen Basin.

The main structural elements interpreted are reverse reactivated basin-bounding normal faults, minor normal faults and a set of strike-slip faults. To assess the structural evolution and fault growth and inversion history in the Mizen Basin, we examined isochore maps between interpreted horizons, key seismic observations and throw-distance (T-x) plots for one of the basin-bounding faults which we consider to be representative of large structures in this area (Figs 5, 8 and 9). Throw measurements include the discrete fault offset and fault-related folding immediately adjacent to the fault (see Yielding and Freeman, 2016, Fig. 10), with throw profiles presented for both the present day throw and the pre-inversion throw on pre-Cenozoic horizons to illustrate the distribution of the original normal fault offsets.

4. Tectonostratigraphic development of the Mizen Basin.

4.1.Structural evolution

In this section we describe the structural evolution of the Mizen Basin with reference to structure contour maps of key horizons, isochore maps of interval thicknesses and selected seismic lines. Table 1 shows a summary of the different units and their corresponding seismic facies and depositional environments.

Our detailed analysis focusses on the main basin-bounding fault (referred to as “Fault A”, Fig. 8). Syn-rift units are preserved in the hanging wall and locally the footwall of this fault with syn-inversion units preserved in its footwall and sometimes its hanging wall. The displacements on this fault have been measured on 6 key horizons (Top Basement, Base Cretaceous unconformity, Base Upper Cretaceous, Base Cenozoic Unconformity, Base Oligocene and Base Miocene). Structural evolution is illustrated on a series of horizon contour maps showing the traces of faults considered to have been active at that time and with throw symbols (normal or reverse) appropriate to that time. This section presents a description of each of the key interpreted intervals with reference to structure contour and thickness maps and to throw vs distance plots (Figs. 10, 11 and 12). These data are interpreted in terms of local structural evolution and kinematics as well as the regional geological evolutionary context at that time.

Pre-Cretaceous

Description

At the base of the pre-Cretaceous succession (Top Basement horizon) two systems of basin bounding faults are observed, labelled FS-A and FS-B (Figs 8 and 10a). These faults are ENE-WSW-striking and NW-dipping and define the two half-grabens that constitute the Mizen Basin. Fault system A is located in the southern part of the Mizen Basin and has a mapped length of 68 km within the study area and a cumulative mapped throw between 500 and 1200 TWTT ms (ca 900m to 2250m) recorded on the top basement horizon (Fig. 12). The fault system at this level consists of two faults (labelled A1 and A2 in Fig. 10) that link through a breached relay ramp. Smaller-scale breached and unbreached relays occur along each of these faults (labelled A11, A21 etc.).

Fault system B, located in the northern part of the Mizen Basin, has a minimum length of 50 km within the study area and a minimum cumulative displacement ranging from 50 ms to 1140 ms TWTT (ca 90m to 2000m) in the northeast and southwest, respectively. It consists of two continuous normal faults (labelled fault B1 and B2, Fig. 8) separated by a relay ramp. Both faults dip towards the NW and have an ENE-WNW strike.

The isochron map of the pre-Cretaceous succession (Fig. 11a) shows maximum thicknesses within two main depocentres. The first depocentre, related to the hanging wall of the FS-A, shows maximum thickness values of 405 ms TWTT (ca 725m) decreasing westwards to 290

ms TWTT (ca 525m). The second depocentre, related to the hanging wall of the fault system B, thickens towards the west and defines two local thickness maxima of 450 and 550 ms TWTT (ca 810m and 1000m) related to the faults B1 and B2 respectively. Finally, in the footwall of FS-A there is a southward and eastward thickening off the Fastnet Spur and into the Fastnet Basin. The more continuous reflector geometries at the top of the pre-Cretaceous section do not suggest significant erosion and the isochore thicknesses are largely depositional.

Throw vs distance plots for FS-A recorded at the base of the pre-Cretaceous succession shows that, at this level, the fault system is composed of two main faults, separated by a relay zone. These faults are labelled FS-A1 and FS-A2 in the Fig. 12a. These throws cannot be calculated accurately for much of fault A1 due to significant footwall erosion in the Middle to Upper Jurassic erosional episode so that the measured values for this fault are minimum estimates.

Interpretation

The pre-Cretaceous stratigraphy in the Mizen Basin is not well known. However, the wedge shaped pre-Cretaceous interval in the hanging-wall of these faults fan and thicken towards FS-A and FS-B (Fig. 1B & C and Fig. 11A) indicating that there was pre-Cretaceous faulting and, by analogy with adjacent areas, the faults were likely to have initiated in the early Triassic times (Fig. 11a-c) and provided accommodation space for deposition of the

Sherwood Sandstone. The timing of fault initiation in this area coincides with the onset of rifting in the adjacent North Celtic Sea and Fastnet basins (Shannon, 1991).

Lower Cretaceous

Description

The lower Cretaceous succession unconformably overlies Jurassic and Triassic strata along the base Cretaceous Unconformity, which is regionally developed in the Celtic Sea basins (Turner, 1995). The Lower Cretaceous comprises the Purbeck Fm. (Berriasian), Wealden Fm. (Valanginian to Aptian) and the basal part of the Greensand Fm. (Albian) (Fig. 5).

The Lower Cretaceous thickness and depocentre distribution broadly follows that of the Pre-Cretaceous succession (Fig. 6) with half-grabens developed in the hanging walls of FS-A and FS-B (Fig. 11b). The hanging wall of FS-A is separated into two depocentres by a local high, one located at the junction between FS-A1 and FS-A2 and the other near the SW termination of the FS-A2. The sequence in the hanging wall of FS-B thins gradually towards the NE mirroring an increase in thickness in the hanging wall of FS-A suggesting transfer of displacement between FS-A and FS-B at this time. The thickness of the lower Cretaceous succession also increases gradually towards the SE margin of the Mizen Basin away from the footwall of FS-A and into the northernmost border of the Fastnet Basin. The minimum thicknesses within the study area are recorded on the Fastnet structural high and the westernmost part of the footwall of the FS-B (Fig. 11b).

The throw vs distance plot for the FS-A at the base Cretaceous succession shows a similar throw distribution as the base of the pre-Cretaceous (Fig. 12a) but the throw values are consistently lower reflecting the throw accrued on these faults in the intervening period and therefore the difference in across-fault thickness of the intervening growth sequence. As above, the throws measured on the base Cretaceous succession for FS-A are minimum estimates where it bounds the Fastnet Spur and its footwall has been subjected possibly to a combination of erosion and non-deposition.

Interpretation

The thickness distribution observed on the isochore map corresponding to the Lower Cretaceous succession (Fig. 11b), shows a period of renewed activity on the pre-Cretaceous fault systems FS-A and FS-B. This is evident from the geometry of the reflectors displayed by the basal lower Cretaceous unit (Purbeck Fm.) which fan out towards the faults in their hanging-walls, away from them in the footwalls and onlap the base Cretaceous unconformity (Fig. 6). This indicates an initial period of subsidence and block rotation controlled by the fault systems FS-A and FS-B during Berriasian to Hauterivian times. The uppermost unit of the Lower Cretaceous succession (Aptian to Barremian) shows a similar pattern but with relatively smaller thickness changes related to the FS-A and FS-B (Fig. 6). These observations suggest that most of the fault activity took place during the early Lower Cretaceous giving rise to the thick depocentres that characterise the Mizen Basin and that fault activity gradually decreased during the late Lower Cretaceous.

Upper Cretaceous

Description

The Upper Cretaceous succession (Fig. 11c) is characterised by a single depocentre located in the northeastern margin of the Mizen Basin, where it reaches maximum thicknesses of 600 ms TWTT (ca 1100m). This succession becomes gradually thinner in all directions but there is a local area of thickening (up to 270 ms TWTT; ca 490m) in the footwall of FS-A which is associated with minor intra-basinal faulting. In this footwall area, the Upper Cretaceous succession gradually pinches out towards the SW beneath the Base Cenozoic unconformity (Fig. 7).

The horizon structure map for the base of this succession (Base Upper Cretaceous, Fig. 8 and Fig. 10c) shows a population of normal faults which strike E-W to NE-SW. These faults include the following: (i) fault segments associated with the reactivated Fs A and B and (ii) relatively minor extensional faults formed during the Upper Cretaceous. The latter are spatially restricted to the footwall of FS-A in the SE margin of the Mizen Basin and to the footwall of the FS-B (Fig. 8). These newly formed faults tip-out upwards in Upper Cretaceous strata (Chalk Group) and are characterised by maximum lengths of 15 km and maximum cumulative displacements of 200 ms TWTT (ca 360m) measured at the base chalk (near Upper Cretaceous) level.

On the Base Upper Cretaceous structure map (Fig. 10c) faults A1 and A2 split into an *en echelon* array of six left-stepping segments, labelled A11 - A13 and A21 - A23. These fault segments parallel the E-W trending faults in the footwall of FS-A. The present day throw on the segmented FS-A at this level (Fig. 12b) varies rapidly along strike with multiple throw null points separating areas of net normal and reverse offset. Backstripping the throws on these faults by removing the later inversion (recorded on the Base Cenozoic; see below) to reconstruct the throws at end Albian times (Fig. 12b) shows that the segmented fault array at this level had a throw of ca. 200 ms (360m) over most of its length and tipped-out towards the east . The throw on each segment decreases towards its lateral terminations and throw is transferred between the segments via a series of relay ramps. Fault throws recorded at the base of the Upper Cretaceous show moderate maximum values (< 250 ms TWTT; < 450m) in comparison with the maximum displacement values recorded in the underlying horizons (> 1000 ms TWTT; > 1800m) (Fig. 12a and b).

Interpretation

Local thickness increases in the hanging wall of both the newly developed normal faults and the basin bounding faults FS-A and B indicate that the faults were active during Late Cretaceous time. The segmentation of the basin bounding faults FS-A combined with the newly developed E-W oriented intra-basinal normal faults are interpreted to indicate a switch of the extension direction from the earlier NW-SE to a N-S orientation. The elevation of the upper tips of the newly developed normal faults indicates that this last phase of extension

lasted until late Cenomanian times, coinciding with the onset of deposition of the Chalk Group (Figs 5 and 6).

Throughout the rest of the Late Cretaceous, post-rift thermal subsidence dominated basin evolution. Although minor across-fault thickness changes could indicate local fault activity with throw values of up to 50 ms TWTT (ca 90m) at that time, the depocentre distribution and the generally flat and onlapping character of reflectors indicate that thermally-driven subsidence was dominant during Late Cretaceous times.

Middle Eocene

Description

The Middle Eocene succession represents the basal part of the syn-inversion stratigraphic sequence. This basal unit (Fig. 11d) is only preserved in the footwall of the FS-A (maximum thickness 110 ms TWTT; ca 200m) and lies unconformably above the Upper Cretaceous succession through the Base Cenozoic unconformity. As in the other Celtic Sea basins there is no lower Eocene to Palaeocene stratigraphy preserved. Two main fault populations are identified to have been active during the deposition of this succession. The first consists of the fault segments A11 - A13 and A21 - A23 related to the fault inversion of the FS-A; at this horizon, these fault segments have reverse throws. The second fault population is a widespread set of NW-SE oriented dextral strike-slip faults (Fig. 10d) across which there are local changes in thickness of the Eocene section.

The throw profiles for FS-A at the base of the syn-inversion sequence (Base Cenozoic in Fig. 12c) demonstrate the transfer of reverse displacement between adjacent fault segments. The aggregate throw profile for all of the segments shows a maximum at the centre of the fault system that decreases systematically towards the east and west. This throw distribution demonstrates that the segments are components of a single kinematic structure (Walsh and Watterson, 1991), as would be expected given the long overlap between them, their close spacing and their linkage into a single structure at depth.

The geometry of the segmented array of reverse faults in FS-A is effectively the same as the array that accommodated extension during the Late Cretaceous (Fig. 12b and c). As in the Late Cretaceous extension, the fault segments are separated by relay ramps that transfer displacement between them so that the extensional relay ramps become inverted and their original dip directions are reversed. This is most clearly seen for the relay zone between A13 and A21 (Fig. 9). A seismic line between segments A13 and A21 (Fig. 9 F-F') shows a distinct eastward-dipping monocline that is the relay ramp connecting the high in the hanging wall to A13 with the footwall of A21. Subtle westward-fanning of seismic reflections between the Base Cenozoic unconformity and the Base Chalk reflects the westward ramp rotation during the extensional phase, with the westward-dipping normal fault of the same age transecting the relay ramp at that time. The individual extensional fault segments were therefore reactivated during inversion and the intervening relay ramps were back-rotated. The

extensional fault that connected A13 and A21was not reactivated during inversion (Fig. 9, section F-F' and Fig. 13).

The NW-SE oriented dextral strike-slip faults affect both the hanging wall and footwall of fault system FS-A. Although they are difficult to identify with certainty on individual cross-sections (Fig. 7) there is no ambiguity in their interpretation as strike-slip faults as they have steep dips, continuous and straight traces on horizon maps (e.g. Base Cenozoic and Base Upper Cretaceous, Fig. 10c, d) and seismic coherence maps (Fig. 8A), and locally have small scale oblique minor faults that step to the left in sympathy with the dextral offset of the main fault. The strongest evidence for a strike-slip origin is that these faults dextrally offset the earlier intrabasinal Late Cretaceous normal faults by as much as 1 km (Fig. 8).

Although the strike-slip faults offset the intra-basinal Upper Cretaceous normal faults, they don't offset the bigger basin bounding faults (Fig. 8), instead the strike-slip faults terminate at the basin-bounding faults. For example, strike-slip faults in the hanging wall of FS-A terminate abruptly against the main fault, which is characterised by a throw vs distance profile showing a stepped geometry where it is intersected by the bigger strike-slip faults (Figs 12b, c and 14). The throw increases across these steps towards the east so that the area immediately east of the branch line (i.e. the intersection line between faults) is a local high, both in terms of the reverse throw on FS-A and the elevation of the associated hanging wall anticline. These observations are consistent with the transfer of lateral offsets on the strike-

slip faults into reverse faulting on the inverted normal faults, a relationship demonstrating that the strike-slip and the inverted faults sets were coeval, for at least part of their growth.

The strike-slip faults affecting the footwall of the Fs-A do not intersect the basin bounding fault but show a progressive northward decrease of lateral offset and appear to tip-out as they approach the basin bounding faults (Figs 11d-f and 14), a feature we later attribute to the asymmetry of deformation either side of inverted faults.

Interpretation

The deposition of this interval above the Base Cenozoic unconformity and spatially restricted to the footwall of the southernmost basin-bounding fault system FS-A indicates that this unit is the first one to be deposited syn-tectonically during the Cenozoic phase of tectonic inversion. The lack of Eocene stratigraphy deposited on the hanging wall of the fault system FS-A (Figs 6 and 11D), suggests this basal sequence was deposited during a period of relatively high rate of inversion assuming there were no major changes in associated sedimentation rates (no significant relative sea-level changes are interpreted from the existing wells). Punctuated thickness increases along these faults at the intersections with NW-SE-striking dextral strike-slip faults (Figs 7 and 11e), suggests that reverse reactivation of normal faults was accompanied by strike-slip faulting during this early stage of inversion.

Oligocene to Lower Miocene

Description

The intermediate unit of the syn-inversion sequence (Fig. 11e) is Oligocene in age and extends over the whole study area. Interval thickness changes dramatically across FS-A with largest thicknesses in the footwall of FS-A indicating continued reverse movement of this structure. Thickness changes across the strike-slip faults is particularly evident in the footwall of the FS-A where a series of elongate depocentres is developed on the eastern side of 4 strike-slip faults. NW – SE oriented depocentres are also present in the hanging wall of the FS-A, where they mark the interaction between the fault segments A13, A21 and A22 and the dextral strike-slip faults.

Throw profiles from the Base Cenozoic horizon (maximum reverse throw of 270 ms TWTT; ca 490m) to the top Oligocene horizon (maximum reverse throw of 50 ms TWTT; ca 90m) show a progressive upward decrease in throw (Fig. 11c to e) demonstrating that reverse movement was ongoing during this interval.

Interpretation

The deposition of Oligocene sediments on both the footwall and hanging wall sides of fault system FS-A records a decrease in fault activity relative to sedimentation rates during this phase of inversion. An increase in the number of depocentres and thickness along the strike-

slip faults (Fig. 7) is accompanied by a decrease in the reverse throw measured in this interval (Fig. 12d).

Lower to Upper Miocene

Description

The uppermost unit of the syn-inversion sequence (Fig. 11f) is distributed over the whole study area with two distinct depocentres: the first located on the western margin of the survey area and the second located in the southeastern part of the study area. Interval thickness increases into the footwalls of both FS-A and B, with minimum thickness values of 130 ms (ca 235m) recorded in their hanging walls. The lateral overlap length between fault segments is lower than on older horizons (Fig. 12c-e) and the relay zones between underlapping segments are often sites of enhanced monoclinal folding.

Interpretation

The significant decrease in fault throw measured at this interval, combined with the reflectors largely overlapping the hanging wall of the fault system FS-A, indicates that by Miocene times the relative rates of inversion and deposition had decreased significantly which is supported by the significant extent of sequence overlap above the inversion structure. Local thickness decreases on the main inversion structures related to the fault segments B1 and A11, A12, A13 and A21, as well as deposition on the flanks of these anticlines, indicate that this phase of inversion was controlled by punctuated growth of the anticlines with an

associated decrease in the amount of reverse faulting (Fig. 11f). No significant depocentres are developed along the strike-slip faults and they do not intersect the Miocene interval (Fig. 7b), features indicating that strike-slip activity had decreased by this time.

5 Discussion

5.1 Structural evolution and regional context

The structural evolution of the Mizen Basin, summarised in Fig. 14, highlights the control of basement structure on all aspects of the tectonic development of the area. The location and orientation of the faults bounding the Triassic basins that formed in response to the first phase of Mesozoic extension in this area followed the trend of Caledonian and/or Variscan basement structures, a configuration that is reminiscent of the relationship observed in onshore Ireland between Caledonian trends and Lower Carboniferous normal faults (e.g. Worthington & Walsh, 2011; Kyne *et al*., 2019). These Triassic faults were subsequently reactivated, initially under NW-SE Early Cretaceous extension and then later under N-S Late Cretaceous extension oblique to deeper structure, leading to the formation of a left-stepping extensional fault system. The segmented character of the normal faults, in turn, defined the geometry of Cenozoic inverted faults and their associated inversion anticlines was arising from renewed reactivation, this time in a reverse sense. The population of dextral strike-slip faults that formed during this inversion event have previously been attributed to the reactivation of Variscan strike-slip faults which, because of their orientation, had been dormant throughout the entire extensional basin history (e.g. Robinson *et al.*, 1981; Petrie *et al.*, 1989). An alternative interpretation is that these are newly formed Cenozoic structures, a model which is consistent with onshore studies suggesting that there is no clear spatial

equivalence between Variscan NW structures and later Cenozoic faults. Nevertheless, it is clear that other important aspects of the Mesozoic structural evolution of the Mizen Basin can be understood in terms of changing stress fields imposed upon Palaeozoic structural fabrics. Here we discuss particular aspects of the structural evolution of the Mizen Basin in the context of observations from the Celtic Sea basins and the wider plate tectonic context.

Pre-Cretaceous basin evolution

The pre-Cretaceous succession in the Mizen Basin is poorly constrained due to a lack of well control. According to our seismic interpretation, the preserved pre-Cretaceous succession is thin (< 600 ms TWT; < 1000m) and comprises dominantly Triassic age sediments deposited during the earliest extensional episode recorded in the basin. As in much of the southwestern domain of the Celtic Sea area, the Jurassic is largely absent (Robinson *et al.*, 1981) in the Mizen Basin due to uplift and erosion, or non-deposition. It is not therefore possible to determine whether the basin underwent the Oxfordian extension recognised in the Celtic Sea basins (Petrie *et al.*, 1989; Shannon, 1991; McMahon & Turner, 1998).

Basement fabric controlling the pattern of faulting and rift geometry of the Celtic Sea basins has been described by several authors (Petrie *et al.*, 1989; Shannon & MacTiernan, 1993; McCann & Shannon, 1994; Rowell, 1995; McCann, 1996), most of whom concluded, from the dominant NE-SW trend, that Caledonian structures control initial basin geometry and orientation. The Mizen Basin, lying on the Variscan thrust terrane, has a dominant ENE-WSW basin orientation which suggests it is controlled by Variscan structures. McCann and Shannon (1994) suggested that the orientation of the Mizen Basin may be the product of the reactivation of Variscan backthrusts which in turn were developed by reactivation of earlier Caledonian structures. This view is supported by the presence of NW-dipping low angle

reflectors previously reported by (McCann & Shannon, 1994) and which are locally identified in the seismic volume used in this study (Fig. 1c).

Cretaceous extensional basin evolution

Although evidence for a Jurassic phase of extension in the Mizen Basin is limited, there is clear evidence for a further rifting stage in Valanginian to Cenomanian times. This time period was characterised by NW – SE oriented extension which caused the reactivation of the NE-SW-striking basin bounding faults. The main extensional phase took place from Valanginian to Barremian times, and was followed by a minor extensional phase recorded from Aptian to Cenomanian, coinciding with a change in orientation of extensional stresses from a NW-SE to a N – S direction. This kinematic history is supported by the E-W-striking intra-basinal normal faults and the segmentation of the basin bounding faults (Fig. 8) showing an associated growth sequence of Aptian to Cenomanian age.

The onset of the third rifting stage is constrained by the oldest Cretaceous stratigraphy preserved in the Mizen Basin, interpreted as Valanginian in age and represented by the Purbeck and Wealden Facies (McCann & Shannon, 1993). The younger reflectors in this unit onlap the Base Cretaceous unconformity (Fig. 6). It is unclear if younger stratigraphy (Berriasian) is preserved within this unit as the 56/12-1 well reaches total depth in Valanginian stratigraphy.

The late Lower Cretaceous extensional phase is represented by newly-formed E-W-striking intra-basinal faults and the segmentation of the basin-bounding faults into E-W and NE-SW-oriented segments. The coherence of this segmentation is supported by displacement-distance (D-x) plots of individual fault segments which together provide aggregate displacements defining a bell-shaped profile typical of a single fault (Fig. 12c). This is consistent with an

interpretation that these segments are kinematically linked, extending downwards into pre-existing NE-SW-striking basin bounding faults which therefore exert a prolonged influence on fault reactivation during the inversion phase.

Since the earliest phase of the third rifting stage recorded in the Mizen Basin in the Early Cretaceous coincides with the timing of active rifting along the Rockall – Hatton margin to the NW of the study area, (Naylor & Shannon, 2011), we interpret both areas to have been influenced by the same NW-SE-extensional stresses. By contrast, the final Aptian extensional phase developed under N-S oriented extension at a time which is broadly coeval with the onset of rifting in the Bay of Biscay (Montadert *et al.*, 1979; Garcia-Mondejar, 1987), also involving a predominantly N-S-direction of extension (Storetvedt, 1972). This Early to Late Cretaceous phase of N-S extension has been observed in other parts of the Celtic Sea basin (Petrie *et al.*, 1989; Rowell, 1995), and we interpret its prevalence to the opening of the Bay of Biscay, which exerted a major influence on the Celtic Sea Basin as rifting in the Rockall Basin declined.

5.2 Timing of inversion

The timing of inversion in the Celtic Sea basins is poorly constrained due to the lack of a preserved syn-inversion stratigraphy. In the Mizen Basin the relatively well preserved Cenozoic section indicates that inversion occurred, either continuously or intermittently, during middle Eocene to late Miocene times with associated co-eval strike-slip faulting. Most of this activity took place during the Oligocene. In common with all of the Celtic Sea basin area, there is no Paleocene section preserved in the Mizen Basin so that it is not possible to establish the timing of the onset of inversion. However, it is possible to place constraints on the amount of pre-Eocene inversion on the basin-bounding fault (FS-A) in the Mizen Basin. Seismic profile F-F’ in Fig. 9 cuts down a relay ramp between two segments of this fault

system as described above. Thickness changes encountered in the section reflect westward ramp rotation during extension, between the Base Chalk and Base Cenozoic, and the opposite sense of rotation towards the east in the Cenozoic section. The middle Eocene section onlaps the ca. 2.5 km long eastward-dipping inversion related ramp suggesting that this structure had some expression before the deposition of the preserved Cenozoic section. The combination of a marked angular unconformity at the crest of the ramp (the base Miocene unconformably lies on the Upper Cretaceous chalk succession) with the preservation of an Eocene section at base of the ramp with only limited erosion of the chalk, suggests that the ramp was developing at this time. Flexural slip restoration of the section shown in Fig. 6 (supplementary material 1) shows that after restoring the section to the Base Cenozoic unconformity, the basin-bounding FS-A fault still has a small reverse throw, suggesting that inversion may have started earlier. Whilst initiation of inversion of FS-A predated the preserved Cenozoic section, inversion was relatively subdued until early Eocene times and may have been inactive during the widespread Paleocene uplift of this region. This observation is in agreement with Le Roy *et al.* (2011) who found that Alpine-related inversion in the Western Approaches initiated during the Ypresian (i.e. lower Eocene) and earlier than the oldest syn-inversion stratigraphy preserved in the Mizen Basin.

5.3 Inversion structures and strain partitioning

Shortening due to inversion in the Mizen Basin was accommodated by a combination of reverse reactivation of the normal faults and associated hanging wall folding and dextral strike-slip faulting. The profiles of reverse throw from the syn-inversion sequence mirror those of the normal throw during earlier extension and the segmented nature of these faults during Cretaceous extension is preserved during reactivation. In addition, the throw profiles

are stepped where they intersect the larger strike-slip faults in the hanging wall with eastward increases in throw across the branchpoints with the dextral strike-slip faults. These displacement and abutment relationships suggest transfer of displacement between the strike-slip faults and the inverted normal faults. Thickness changes within the syn-inversion sequences and the elevations of strike-slip tip-lines indicate that the inversion and strike-slip faulting occurred within the same broad time interval, with the transfer of displacement between them demonstrating that they were active at the same time. In contrast to the strike-slip faults in the hanging wall of FS-A, those in the footwall do not intersect the inverted normal faults but rather they terminate before they intersect the FS-A. The strike-slip faults are generally not aligned across the FS-A and we conclude that they were never continuous across it. The reason for the difference in behaviour of the strike-slip faults across the FS-A is unclear but may be related to the asymmetry in inversion-related folding, with large hanging wall buttress folds but little or no folding in the footwall, a characteristic feature of inverted normal faults (Bonini *et al.*, 2012). Irrespective of their precise kinematics, it is clear from this configuration that the strike-slip faults were active during the inversion of the normal faults.

Compression in the brittle field can be accommodated by reverse faults and/or by conjugate strike slip faults, and reverse and strike-slip faulting are often developed in association with each other. For example, tear faults transfer displacements between thrusts and strains within transpressional zones can be partitioned onto reverse and strike-slip structures (Cunningham

& Mann, 2007). The structural arrangement in the Mizen Basin is somewhat unusual with two synchronous fault systems at a relatively high angle to each other (45-70^0), one reverse and one strike-slip, with both combining to accommodate shortening.

There are occasional minor sinistral strike-slip faults in the footwall of the SF-A (Fig. 8) and these define a conjugate system with the dextral faults about an approximately N-S median line. This relationship indicates formation under a broadly N-S compression direction consistent with the overall trend of Alpine-related inversion structures in this region (Murdoch et al. 1995). The basin bounding normal faults strike c. 070 and are slightly oblique to the compression direction introducing a sinistral transpressive component of strain which is likely to be accommodated by oblique slip on the reactivated normal faults. The dextral strike-slip faults could either be newly formed in response to N-S compression or arise from the presence of similarly oriented structures in the basement. The optimally-oriented sinistral conjugate fault set is poorly developed because this component of offset is accommodated on the inverted normal faults. The Mizen Basin therefore provides an example of partitioning of contractional strains onto near-orthogonal sets of different fault modes due to the existence of pre-existing structure.

5.4 Comparison with surrounding areas

While inversion of earlier normal faults is the primary response to Alpine-Pyrenean inversion in the Celtic Sea basins and throughout the southern part of Ireland and Britain, the spatio-temporal relationship of strike-slip faults and normal fault inversion varies between areas. In

the Bristol Channel Basin, for example, Alpine deformation produced dextral strike-slip faults that have previously been considered to post-date the inversion of normal faults (Williams *et al.*, 2005), perhaps suggesting the increasing importance of strike-slip faulting with time. A similar geometrical configuration is also seen in the Irish Sea, with newly-formed NNW-trending dextral strike-slip faults, accommodating displacements of up to ca 9km (e.g. the Codling Fault; Anderson et al. 2018), combining with the inversion of pre-existing normal faults, of Permo-Triassic and possibly Carboniferous age, involving sinistral transpression (i.e. compression and sinistral strike-slip displacements). Outcrop and mine studies, together with newly acquired aeromagnetic Tellus dataset in Ireland's onshore, also highlight the prevalence of ubiquitous newly formed NNW-trending dextral strike-slip faults (Carboni *et al.*, 2003; Fusciardi *et al.*, 2003; Moore & Walsh, 2013) and the development of more localised Cenozoic sinistral strike-slip fault displacement (up to 2.5km) on pre-existing Carboniferous normal faults. This conjugate configuration of faults has been attributed to two principal phases of Alpine-Pyrenean deformation, one in the Early Palaeocene or Late Cretaceous, and another in the Oligocene (Cooper *et al.*, 2012; Anderson *et al.*, 2016; Anderson *et al.*, 2018): given the absence of additional temporal constraints (e.g. fault-related sedimentation or offset volcanic/magmatic bodies) other phases cannot, however, be ruled out. The work of this study broadly confirms the basic configuration of deformation seen across Ireland, with a preponderance of NW- and NNW-trending dextral strike-slip faults combining with inverted normal faults which are predominantly reverse when they are E-W

trending, but which accommodate an increasing component of sinistral strike-slip movement as they become more NE-trending. We cannot from our data demonstrate the presence of pre-existing NW-SE trending basement structures which may localise later dextral faults in the study area, as suggested by other authors (Robinson *et al.*, 1981; Petrie *et al.*, 1989), work in other areas indicates that approximately N-S inversion is often accommodated by synchronous movement on newly formed NW- and NNW-striking dextral faults and pre-existing NE- to E-trending normal faults.

5. Summary and conclusions

This study provides an improved understanding of the timing and style of inversion structures in the Celtic Sea Basins capitalising on the recent acquisition and analysis of a 3D seismic dataset that images the very well-preserved Mesozoic to Cenozoic sequence in the Mizen Basin.

The main features of the Mesozoic and Cenozoic structural development of the Mizen Basin were controlled by reactivation of Palaeozoic structures (Caledonian and Variscan) in extension, contraction or strike-slip movement arising from deformation phases linked to changing stress field orientations. The basin bounding faults were active in NW-SE oriented extension from Triassic to Lower Cretaceous times to produce the two half-graben depocentres that characterise the Mizen Basin. From late Lower to early Upper Cretaceous (Valanginian to Cenomanian) times the extension direction of the Mizen Basin became oriented N-S, leading to segmentation of pre-existing basin bounding faults and the formation of E-W-striking intra-basinal normal faults.

After a period of widespread Paleocene uplift with no sedimentary record preserved, basin inversion occurred from Middle Eocene to Miocene. There is no evidence that the Paleocene

uplift was accompanied by reactivation, either positive or negative, of the earlier faults. This observation suggests that the Paleocene uplift was epeirogenic rather than related to tectonic inversion.

Cenozoic inversion in the Mizen Basin occurred by a combination of reverse reactivation of Mesozoic extensional faults and dextral offset along NW-SE trending strike-slip faults that show synchronous activity for at least part of their growth histories. This combination of structures that partition N-S shortening onto different faulting modes, developed primarily because pre-existing Palaeozoic structures, mainly with ENE-trending strikes, were preferentially reactivated.

Inversion-related reverse displacements on basin bounding faults often mirrors their pre-existing normal displacement distributions associated with Cretaceous extension. The pattern of normal fault segments and, in at least one case, the relay ramps, is reactivated during inversion, to partly define the locations of hanging wall anticlines. Relay ramps between normal fault segments are back-rotated during inversion and play a key role in controlling the geometries of later inversion anticlines. The location of inversion structures is related to the geometry of the earlier extensional faults, with the geometry and closure of associated, relatively asymmetric, traps defined by a combination of buttressing, reverse reactivation and strike-slip faulting.

Acknowledgements:

We gratefully acknowledge the Petroleum Affairs Division (PAD) of the Department of Communications, Climate Action and Environment (DCCAE) for providing the data used in this project and the permission to show the seismic profiles. Schlumberger Oilfield UK Plc. are thanked for providing Petrel software and Badley Geoscience Ltd for T7. We also thank the Petroleum Infrastructure Programme (PIP) for co-funding this research. C.Childs is funded by Tullow Oil. This publication has emanated from research supported in part by a research grant from Science Foundation Ireland (SFI) under Grant Number 13/RC/2092 and co-funded under the European Regional Development Fund and by PIPCO RSG and its member companies. The authors declare that there is no conflict of interest regarding the publication of this article.

References

ANDERSON, H., WALSH, J.J. & COOPER, M. (2016) Faults, Intrusions and Flood Basalts: The Cenozoic Structure of the North of Ireland. In: Unearthed: Impacts of the Tellus Surveys of the North of Ireland. (Ed. by Young, M.E.). Royal Irish Academy, Dublin, 180-189. DOI:10.3318/978-1-908996-88-6.ch14.

ANDERSON, H., WALSH, J.J. & COOPER, M.R. (2018) The Development of a Regional-Scale Intraplate Strike-Slip Fault System; Alpine Deformation in the North of Ireland. *Journal of Structural Geology*, **116,** 47-63.

ANELL, I., THYBO, H. & ARTEMIEVA, I. (2009) Cenozoic Uplift and Subsidence in the North Atlantic Region: Geological Evidence Revisited. *Tectonophysics*, **474,** 78-105.

BALLY, A.W. (1984) Tectogenese Et Sismique Reflexion. *Bulletin de la Société Géologique de France*, **S7-XXVI,** 279-285.

BARR, K., COLTER, V. & YOUNG, R. (1981) The Geology of the Cardigan Bay-St. George's Channel Basin. *Petroleum geology of the continental shelf of North-West Europe***,** 432-443.

BIRPS & ECORS (1986) Deep Seismic Reflection Profiling between England, France and Ireland. *Journal of the Geological Society*, **143,** 45-52.

BONINI, M., SANI, F. & ANTONIELLI, B. (2012) Basin Inversion and Contractional Reactivation of Inherited Normal Faults: A Review Based on Previous and New Experimental Models. *Tectonophysics*, **522,** 55-88.

BUCHANAN, J.G. & BUCHANAN, P.G. (1995) *Basin Inversion*. Geological Society London.

CARBONI, V., WALSH, J., STEWART, D., GÜVEN, J. & ELIOPOULOS, D. (2003). *Timing and Geometry of Normal Faults and Associated Structures at the Lisheen Zn-Pb Deposit, Ireland–Investigating Their Role in the Transport and the Trapping of Metals*. Mineral Exploration and Sustainable Development: Proceedings of the 7th Biennial SGA Meeting.

CASTON, V., DEARNLEY, R., HARRISON, R., RUNDLE, C. & STYLES, M. (1981) Olivine-Dolerite Intrusions in the Fastnet Basin. *Journal of the Geological Society*, **138,** 31-46.

CASTON, V. (1995) The Helvick Oil Accumulation, Block 49/9, North Celtic Sea Basin. *Geological Society, London, Special Publications*, **93,** 209-225.

CHEADLE, M., MCGEARY, S., WARNER, M. & MATTHEWS, D. (1987) Extensional Structures on the Western Uk Continental Shelf: A Review of Evidence from Deep Seismic Profiling. *Geological Society, London, Special Publications*, **28,** 445-465.

COLIN, J., LEHMANN, R. & MORGAN, B. (1981) Cretaceous and Late Jurassic Biostratigraphy of the North Celtic Sea Basin, Offshore Southern Ireland. *Microfossils from Recent and fossil shelf seas***,** 122-155.

COOPER, M., ANDERSON, H., WALSH, J., VAN DAM, C., YOUNG, M., EARLS, G. & WALKER, A. (2012) Palaeogene Alpine Tectonics and Icelandic Plume-Related Magmatism and Deformation in Northern Ireland. *Journal of the Geological Society*, **169,** 29-36.

COWARD, M. (1983) Thrust Tectonics, Thin Skinned or Thick Skinned, and the Continuation of Thrusts to Deep in the Crust. *Journal of Structural Geology*, **5,** 113-123.

CRAVEN, J.E. (1995) The Tectonic Evolution, Stratigraphy and Petroleum Potential of the Mizen Basin, Southwest Celtic Sea. *Geological Society, London, Special Publications*, **93,** 277-277.

CUNNINGHAM, W. & MANN, P. (2007) Tectonics of Strike-Slip Restraining and Releasing Bends. *Geological Society, London, Special Publications*, **290,** 1-12.

DEWEY, J.F., HOLDSWORTH, R.E., STRACHAN, R.A., 1998. Transpressionand transtension zones. In: Holdsworth, R.E., Strachan, R.E.,Dewey, J.F. (Eds.), Continental Transpressional andTranstensional Tectonics. Geological Society of London Special Publication 135, pp 1-14

DORÉ, A. & LUNDIN, E. (1996) Cenozoic Compressional Structures on the Ne Atlantic Margin; Nature, Origin and Potential Significance for Hydrocarbon Exploration. *Petroleum Geoscience*, **2,** 299-311.

DORÉ, A., CARTWRIGHT, J., STOKER, M., TURNER, J. & WHITE, N. (2002) Exhumation of the North Atlantic Margin: Introduction and Background. *Geological Society, London, Special Publications*, **196,** 1-12.

FUSCIARDI, L., GUVEN, J., STEWART, D., CARBONI, V. & WALSHE, J. (2003) The Geology and Genesis of the Lisheen Zn-Pb Deposit, Co. Tipperary, Ireland. *Europe's major base metal deposits: Dublin, Irish Association for Economic Geology***,** 455-481.

GABRIELSEN, R., GRUNNALEITE, I. & OTTESEN, S. (1993) Reactivation of Fault Complexes in the Loppa High Area, Southwestern Barents Sea. In: *Norwegian Petroleum Society Special Publications* (Ed. by, **2**, 631-641. Elsevier.

GARCIA-MONDEJAR, J. (1987) Aptian-Albian Carbonate Episode of Basque-Cantabrian Basin, Northern Spain. *AAPG (Am. Assoc. Pet. Geol.) Bull.;(United States)*, **71**.

GARDINER, P.R. (1970) Regional Fold Structures in the Lower Palaeozoics of South-East Ireland. *Bulletin of the Geological Survey of Ireland*, **1,** 47-51.

GARDINER, P.R. & SHERIDAN, D.J. (1981) Tectonic Framework of the Celtic Sea and Adjacent Areas with Special Reference to the Location of the Variscan Front. *Journal of Structural Geology*, **3,** 317-331.

GILL, W. D. (1962) The Variscan fold belt in Ireland. In: Some Aspects of the Variscan Fold Belt (Ed. By K. Coe), 49-64. Manchester University Press.

GLENNIE, K. & BOEGNER, P. (1981) Sole Pit Inversion Tectonics. *Petroleum geology of the continental shelf of northwest Europe. Institute of Petroleum, London***,** 110-120.

HARDING, T. (1985) Seismic Characteristics and Identification of Negative Flower Structures, Positive Flower Structures, and Positive Structural Inversion. *AAPG Bulletin*, **69,** 582-600.

HITZMAN, M.W. (1999) Extensional Faults That Localize Irish Syndiagenetic Zn-Pb Deposits and Their Reactivation During Variscan Compression. *Geological Society, London, Special Publications*, **155,** 233-245.

JONES, R. R., & TANNER, P. G. (1995) Strain partitioning in transpression zones. Journal of Structural Geology, **17(6)**, 793-802.

LE ROY, P., GRACIA-GARAY, C., GUENNOC, P., BOURILLET, J.-F., REYNAUD, J.-Y., THINON, I., KERVEVAN, P., PAQUET, F., MENIER, D. & BULOIS, C. (2011) Cenozoic Tectonics of the Western Approaches Channel Basins and Its Control of Local Drainage Systems. *Bulletin de la Société Géologique de France*, **182,** 451-463.

MCCANN, T. & SHANNON, P. (1993) Lower Cretaceous Seismic Stratigraphy and Fault Movement in the Celtic Sea Basin, Ireland. *First Break*, **11,** 335-344.

MCCANN, T. & SHANNON, P.M. (1994) Late Mesozoic Reactivation of Variscan Faults in the North Celtic Sea Basin, Ireland. *Marine and petroleum geology*, **11,** 94-103.

MCCANN, T. (1996) The North Celtic Sea Reflector—a Possible Caledonian Basement Structure, Offshore Southern Ireland. *Tectonophysics*, **266,** 361-377.

MCGEARY, S., CHEADLE, M., WARNER, M., BLUNDELL, D., BROOKS, J. & GLENNIE, K. (1987) Crustal Structure of the Continental Shelf around Britain Derived from Birps Deep Seismic Profiling. *Petroleum Geology of North West Europe*, **1,** 33-41.

MCMAHON, N.A. & TURNER, J. (1998) The Documentation of a Latest Jurassic-Earliest Cretaceous Uplift Throughout Southern England and Adjacent Offshore Areas. *Geological Society, London, Special Publications*, **133,** 215-240.

MENPES, R.J. & HILLIS, R.R. (1995) Quantification of Tertiary Exhumation from Sonic Velocity Data, Celtic Sea/South-Western Approaches. *Geological Society, London, Special Publications*, **88,** 191-207.

MILLER, K.G., KOMINZ, M.A., BROWNING, J.V., WRIGHT, J.D., MOUNTAIN, G.S., KATZ, M.E., SUGARMAN, P.J., CRAMER, B.S., CHRISTIE-BLICK, N. & PEKAR, S.F. (2005) The Phanerozoic Record of Global Sea-Level Change. *Science*, **310,** 1293-1298.

MONTADERT, L., DE CHARPAL, O., ROBERTS, D., GUENNOC, P. & SIBUET, J.C. (1979) Northeast Atlantic Passive Continental Margins: Rifting and Subsidence Processes. *Deep Drilling Results in the Atlantic Ocean: Continental Margins and Paleoenvironment***,** 154-186.

MOORE, J. & WALSH, J. (2013) Analysis of Fracture Systems and Their Impact on Flow Pathways in Irish Bedrock Aquifers. *Geological Survey of Ireland Groundwater Newsletter*, **51,** 28-33.

MURDOCH, L., MUSGROVE, F. & PERRY, J. (1995) Tertiary Uplift and Inversion History in the North Celtic Sea Basin and Its Influence on Source Rock Maturity. *Geological Society, London, Special Publications*, **93,** 297-319.

NAYLOR, D. (1978) A Structural Section across the Variscan Fold Belt, Southwest Ireland. *Journal of Earth Sciences***,** 63-70.

NAYLOR, D. & SHANNON, P.M. (1982) *Geology of Offshore Ireland and West Britain*, 1 edn. Springer Netherlands.

NAYLOR, D. & SHANNON, P.M. (2011) *Petroleum Geology of Ireland*. Dunedin Academic Press Limited.

PETRIE, S.H., BROWN, J.R., GRANGER, P.J. & LOVELL, J.P.B. (1989) Mesozoic History of the Celtic Sea Basins. In: *Extensional Tectonics and Stratigraphy of the North Atlantic Margins* (Ed. by A. J. Tankard & H. R. Balkwill). American Association of Petroleum Geologists.

PHARAOH, T.C. (1996) *Tectonic Map of Britain, Ireland and Adjacent Areas: Sheet 1*. British Geological Survey.

PINET, B., MONTADERT, L., MASCLE, A., CAZES, M. & BOIS, C. (1987) New Insights on the Structure and the Formation of Sedimentary Basins from Deep Seismic Profiling in Western Europe. *Petroleum geology of north west Europe*, **1,** 11-31.

PRAEG, D., STOKER, M., SHANNON, P., CERAMICOLA, S., HJELSTUEN, B., LABERG, J. & MATHIESEN, A. (2005) Episodic Cenozoic Tectonism and the Development of the Nw European 'Passive'continental Margin. *Marine and Petroleum Geology*, **22,** 1007-1030.

RIIS, F., VOLLSET, J. & SAMD, M. (1986) Tectonic Development of the Western Margin of the Barents Sea and Adjacent Areas. In: Future Petroleum Provinces of the World (Ed. by M.T. Halbouty), vol. 40, pp. 661-675. AAPG Memoir (1986)

ROBERTS, D. (1989) Basin Inversion in and around the British Isles. *Geological Society, London, Special Publications*, **44,** 131-150.

ROBINSON, K., SHANNON, P. & YOUNG, D. (1981) The Fastnet Basin: An Integrated Analysis. *Petroleum geology of the continental shelf of north-west Europe. Heyden, London***,** 444-454.

ROWELL, P. (1995) Tectono-Stratigraphy of the North Celtic Sea Basin. *Geological Society, London, Special Publications*, **93,** 101-137.

SHANNON, P. (1979) The Tectonic Evolution of the Lower Palaeozoic Rocks of Extreme Se Ireland. *Geological Society, London, Special Publications*, **8,** 281-285.

SHANNON, P. (1991) Tectonic Framework and Petroleum Potential of the Celtic Sea, Ireland. *First Break*, **9**.

SHANNON, P. (1991) The Development of Irish Offshore Sedimentary Basins. *Journal of the Geological Society*, **148,** 181-189.

SHANNON, P. & MACTIERNAN, B. (1993) Triassic Prospectivity in the Celtic Sea, Ireland-a Case History. *First Break*, **11,** 47-57.

SIBUET, J.C., DYMENT, J., BOIS, C., PINET, B. & ONDREAS, H. (1990) Crustal Structure of the Celtic Sea and Western Approaches from Gravity Data and Deep Seismic Profiles: Constraints on the Formation of Continental Basins. *Journal of Geophysical Research: Solid Earth*, **95,** 10999-11020.

ŠTOLFOVÁ, K. & SHANNON, P.M. (2009) Permo-Triassic Development from Ireland to Norway: Basin Architecture and Regional Controls. *Geological Journal*, **44,** 652-676.

STORETVEDT, K. (1972) Crustal Evolution in the Bay of Biscay. *Earth and Planetary Science Letters*, **17,** 135-141.

STUEVOLD, L.M. & ELDHOLM, O. (1996) Cenozoic Uplift of Fennoscandia Inferred from a Study of the Mid-Norwegian Margin. *Global and Planetary Change*, **12,** 359-386.

TABER, D., VICKERS, M. & WINN, R. (1995) The Definition of the Albian 'A'sand Reservoir Fairway and Aspects of Associated Gas Accumulations in the North Celtic Sea Basin. *Geological Society, London, Special Publications*, **93,** 227-244.

TAPPIN, D.R., CHADWICK, R.A., JACKSON, A.A., WINGFIELD, R.T.R., & SMITH, N.J.P. (1994) United Kingdom offshore regional report: The geology of Cardigan Bay and the Bristol Channel. London HMSO for the British Geological Survey, 107pp.

TESÓN, E., MORA, A., SILVA, A., NAMSON, J., TEIXELL, A., CASTELLANOS, J., CASALLAS, W., JULIVERT, M., TAYLOR, M., IBÁÑEZ-MEJÍA, M. & VALENCIA, V.A. (2013) Relationship of Mesozoic Graben Development, Stress, Shortening Magnitude, and Structural Style in the Eastern Cordillera of the Colombian Andes. *Geological Society, London, Special Publications*, **377,** 257-283.

TIKOFF, B., & TEYSSIER, C. (1994) Strain modeling of displacement-field partitioning in transpressional orogens. Journal of Structural Geology, **16(11)**, 1575-1588.

TURNER, J.P. & WILLIAMS, G.A. (2004) Sedimentary Basin Inversion and Intra-Plate Shortening. *Earth-Science Reviews*, **65,** 277-304.

VÅGNES, E., GABRIELSEN, R. & HAREMO, P. (1998) Late Cretaceous–Cenozoic Intraplate Contractional Deformation at the Norwegian Continental Shelf: Timing, Magnitude and Regional Implications. *Tectonophysics*, **300,** 29-46.

WALSH, J. J., & WATTERSON, J. (1991) Geometric and kinematic coherence and scale effects in normal fault systems. Geological Society, London, Special Publications, **56**, 193-203.

WILLIAMS, G., POWELL, C. & COOPER, M. (1989) Geometry and Kinematics of Inversion Tectonics. *Geological Society, London, Special Publications*, **44,** 3-15.

WILLIAMS, G.A., TURNER, J.P. & HOLFORD, S.P. (2005) Inversion and Exhumation of the St. George's Channel Basin, Offshore Wales, Uk. *Journal of the Geological Society*, **162,** 97-110.

WORTHINGTON, R. & WALSH, J.J. (2011) Structure of Lower Carboniferous basins of NW Ireland, and its implications for structural inheritance and Cenozoic faulting. *Journal of Structural Geology*, **33**, 1285-1299.

YIELDING, G., & FREEMAN, B. (2016) 3-D seismic-structural workflows - examples using the Hat Creek fault system. In: 3-D Structural Interpretation: Earth, Mind, and Machine (Ed. by B. Krantz, C. Ormand, B. Freeman), vol. 111 , pp. 155-171. AAPG Memoir (2016)

ZIEGLER, P. (1987) Celtic Sea-Western Approaches Area: An Overview. *Tectonophysics*, **137,** 285-289.

ZIEGLER, P. (1990a). *Geological Atlas of Western and Central Europe*, Geological Society of London.

ZIEGLER, P. (1990b) Collision Related Intra-Plate Compression Deformations in Western and Central Europe. *Journal of Geodynamics*, **11,** 357-388.

Formation/interval		Seismic facies	Depositional environment
Post-Inversion 2		continuous, medium amplitude and medium frequency reflectors	shallow marine deposits
Post-Inversion 1		discontinuous, low amplitude and high frequency reflectors	shallow marine deposits
Syn-Inversion 3	**b**	continuous, medium amplitude and high frequency reflectors	inner sublittoral and littoral environment
	a	continuous, medium amplitude and medium frequency reflectors	outer littoral environment
Syn-Inversion 2	**b**	continuous, medium amplitude and medium frequency reflectors	deepening upwards inner to outer sublittoral environment.
	a	poorly continuous medium amplitude and medium frequency reflectors	
Syn-Inversion 1		highly continuous, low amplitude and medium frequency reflectors	high energy marine, inner sublittoral environment
Chalk		poorly continuous, medium amplitude and high frequency reflectors	middle shelf deposits
Greensand		continuous, medium amplitude and medium frequency reflectors	middle shelf deposits.
Wealden	**b**	continuous, medium amplitude and medium to high frequency reflectors	shallow marine shelf deposits
	a	poorly continuous, high amplitude and medium frequency reflectors	fluvial channel and overbank deposits
Purbeck		poorly continuous, low to medium frequency and medium amplitude reflectors	brackish to marginal marine environment
Pre-Cretaceous	**Jurassic**	poorly continuous, low amplitude and high frequency reflectors	pro-delta mudstones
	Triassic	poorly continuous, high amplitude and low frequency reflectors	continental fluvial channelized sandstones

Table 1. Seismic facies and depositional environment of the interpreted units. The discontinuous lines represent the interpreted horizons.

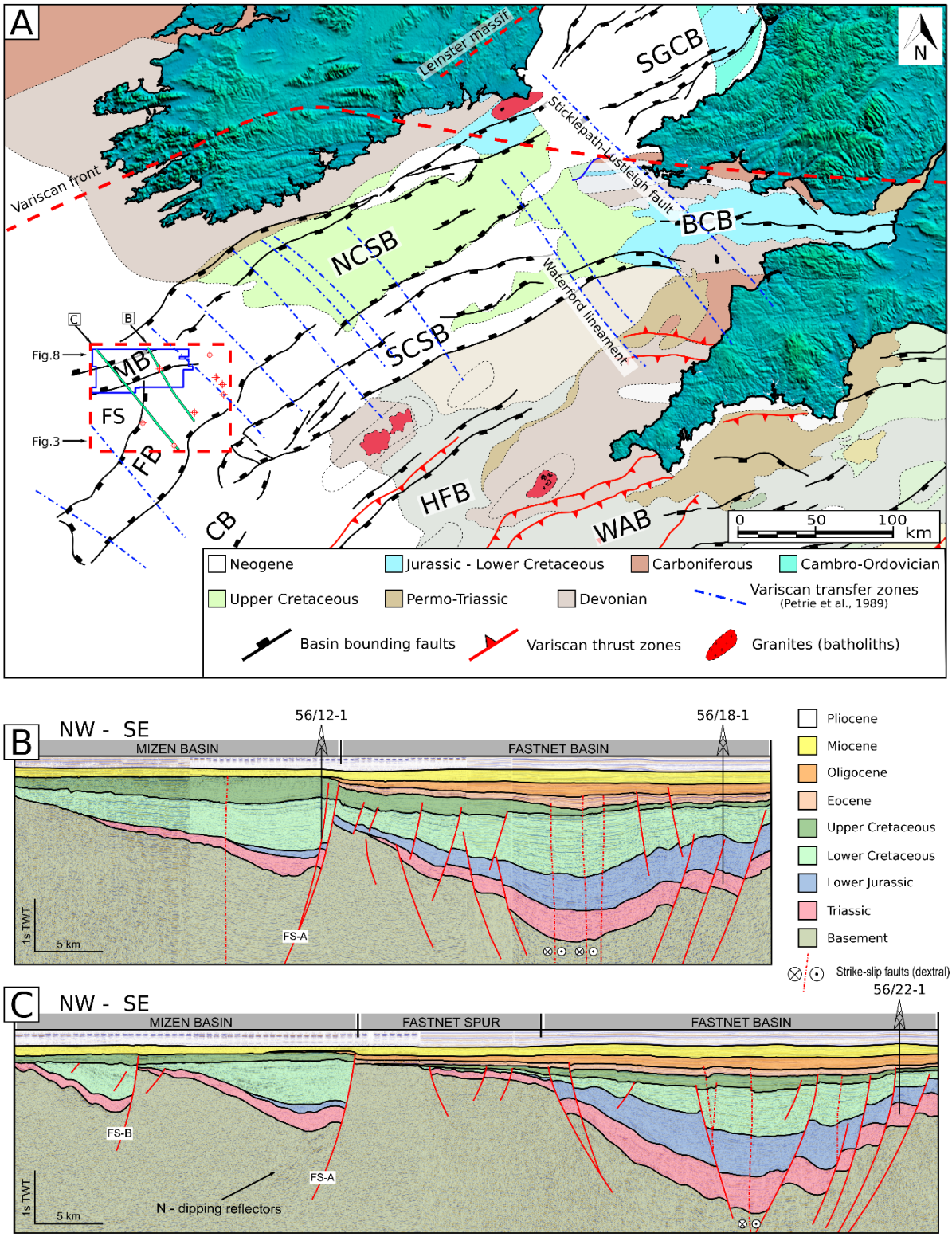

Figure 1. (a) Map showing the main structural elements of the Celtic Sea Basins and sea-floor subcrop map of the main lithological ages. The subcrop map has been modified from Pharaoh, T. C. (1996) whereas the structural elements have been modified from Shannon, P. (1991). The red box indicates the location of the study area. (b) and (c) Representative cross-sections of the Mizen and Fastnet basins based on the interpretation of two composite seismic lines.

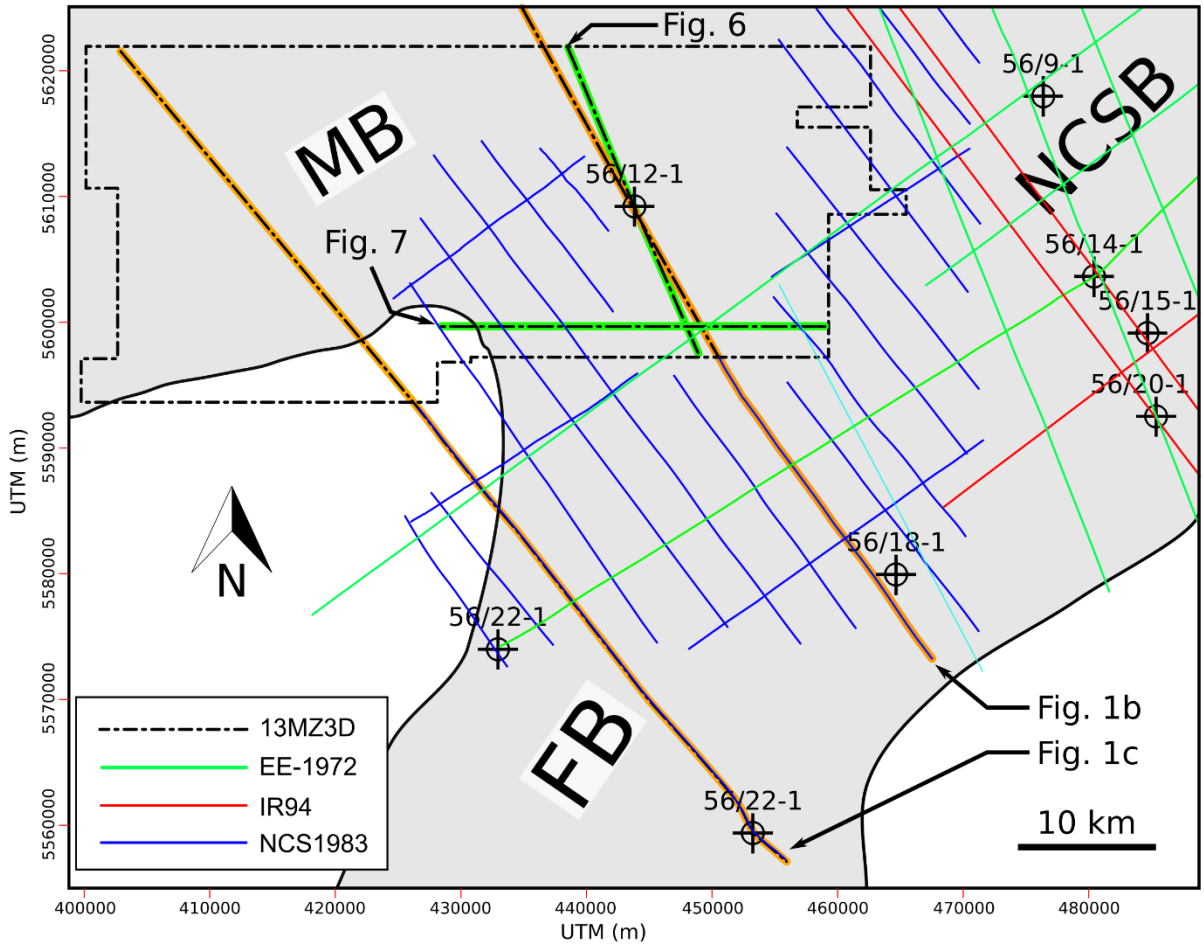

Figure 2. Map showing the location of the 3D seismic reflection survey (13MZ3D), 2D seismic lines from three 2D surveys (see key), two composite seismic lines (Fig. 1b and c), random lines (Figs. 6 and 7) and the main wells used in this study. The location of this map is shown within the red square in the Fig. 1a.

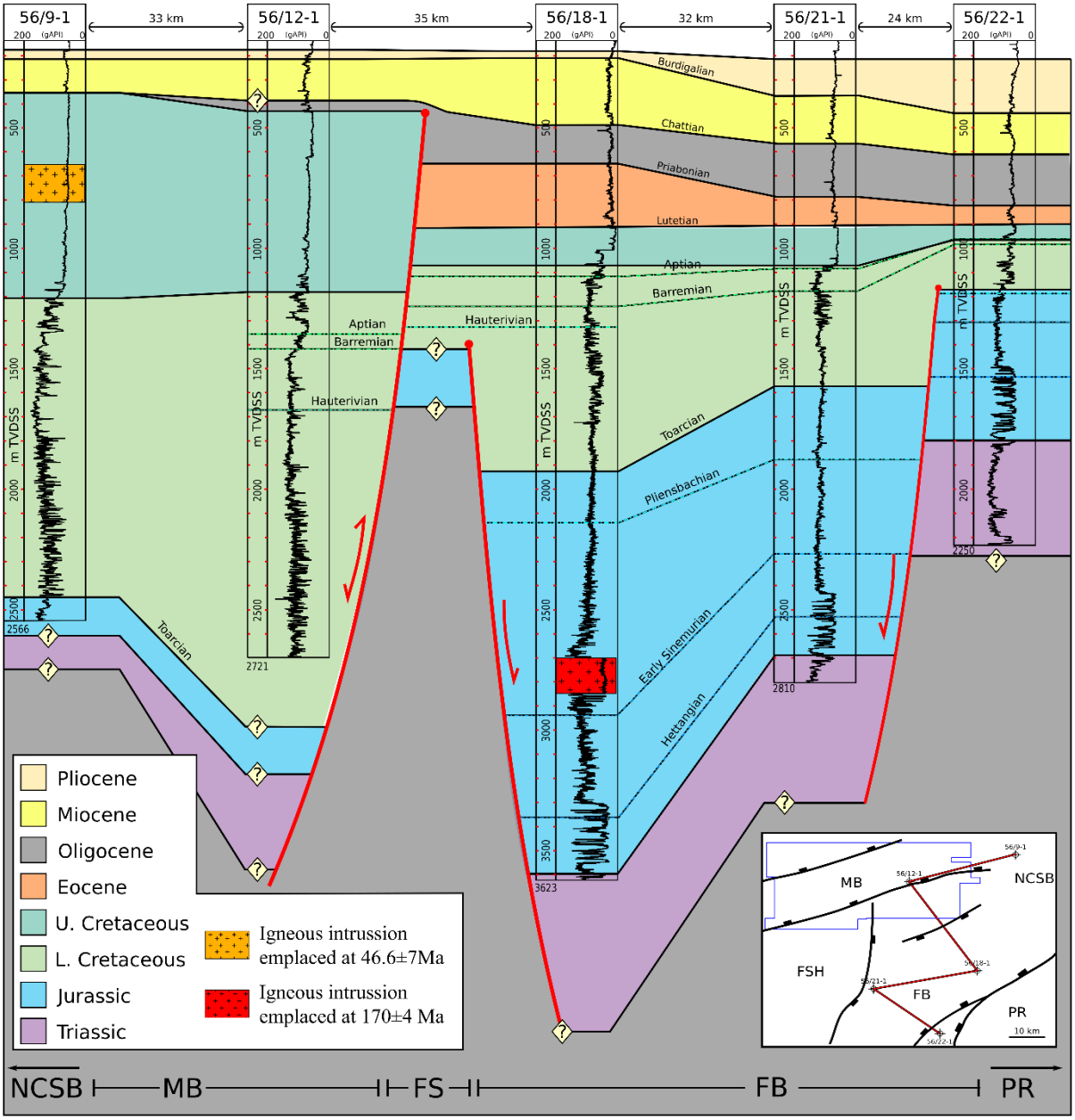

Figure 3. Stratigraphic correlation of the Miocene to Lower Jurassic succession along the southernmost boundary of the North Celtic Sea Basin (Well 56/9-1), the Mizen Basin (Well 56/12-1) and the northernmost boundary of the Fastnet Basin (wells 56/18-1 and 56/22-1). The age of cooling of the igneous intrusions is based on K-Ar dating available in the well reports. For the well location see Fig. 2. The basins are separated by basement highs, the Fastnet Spur (FS) and the Labadie-Bank/Pembrokeshire Ridge (PR).

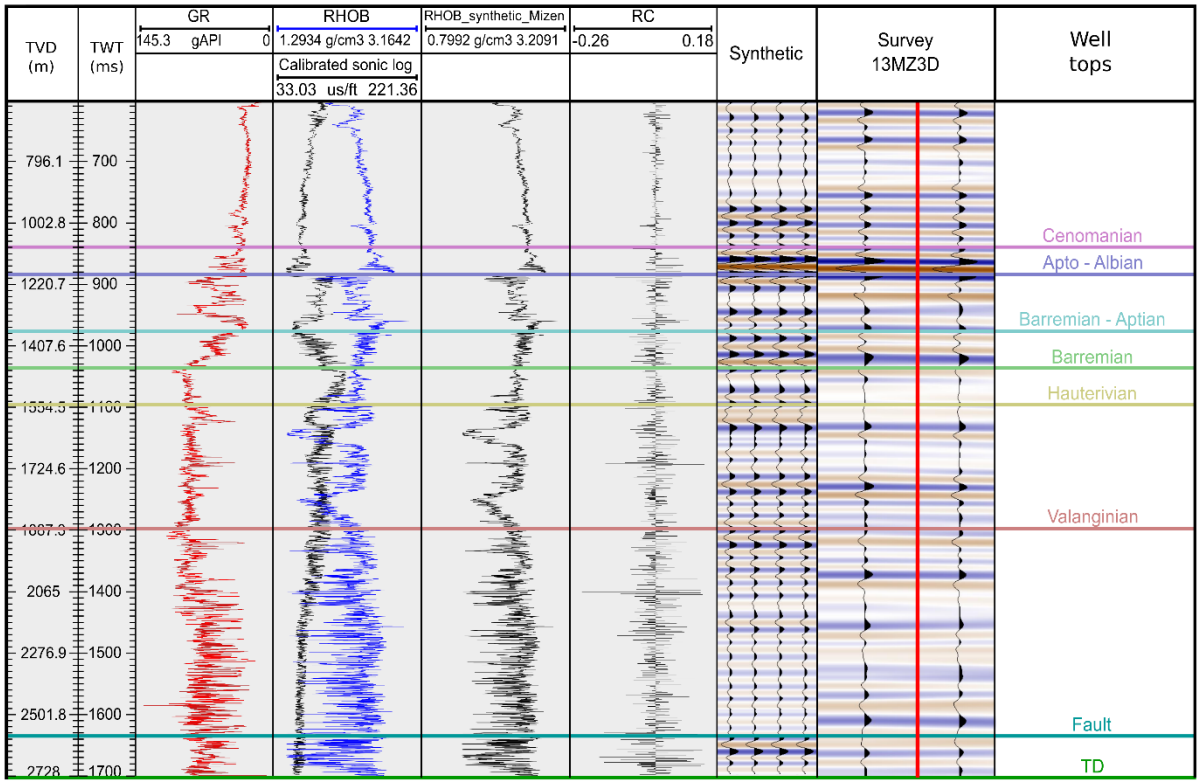

Figure 2. Wireline log data and seismic well-ties for the well 56/12-1 and interpreted horizons. The well location is shown on the Fig. 3. A negative reflection coefficient is represented by a positive number and as a peak (blue colour on display), positive reflection coefficient is represented by a negative number and as a trough (red colour on display).

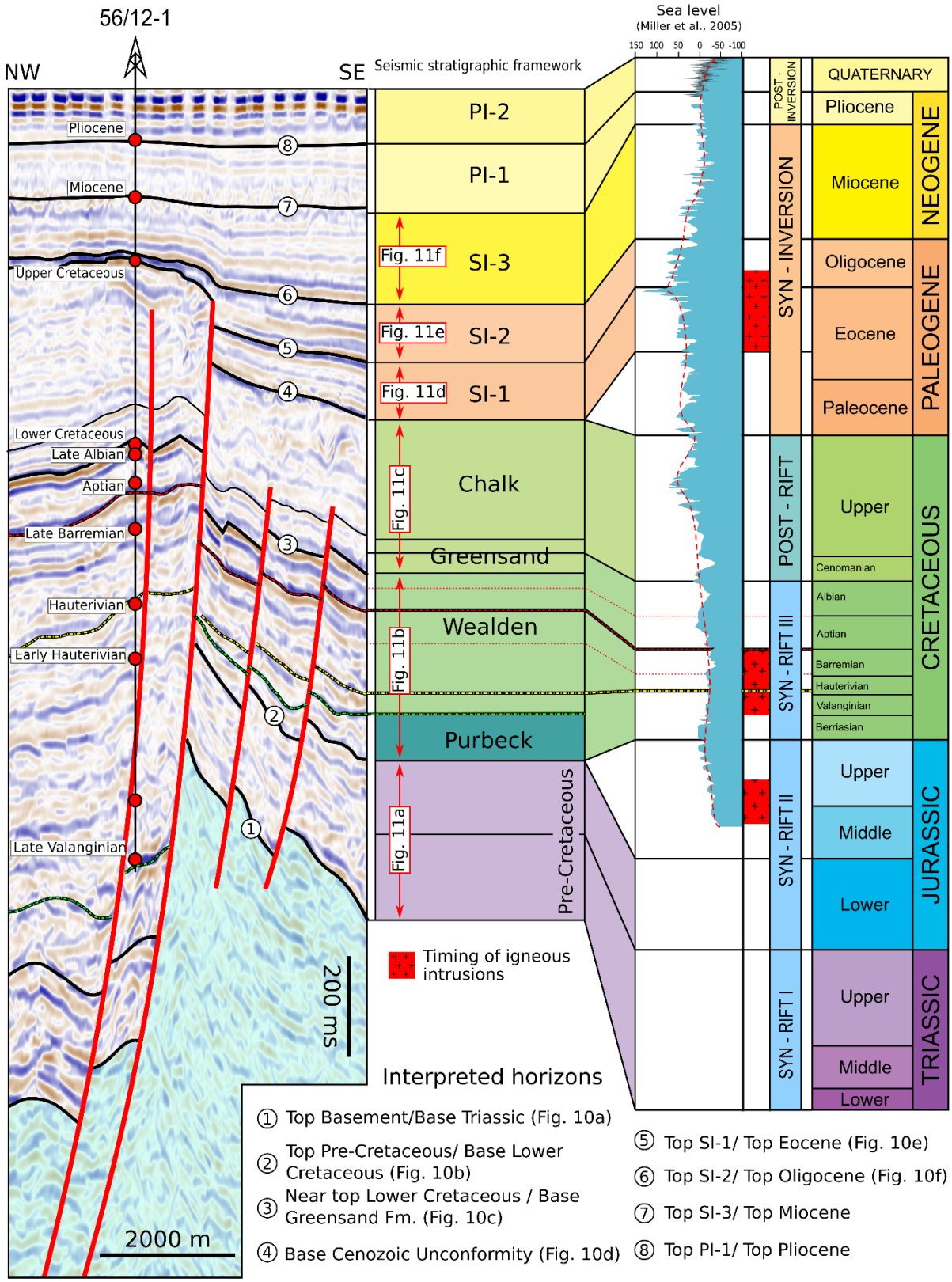

Figure 3. Seismic panel through the 56/12-1 well and the stratigraphic framework showing the formations age within the Mizen Basin. The interpreted horizons are based on the synthetic seismogram of the well 56/12-1 (Fig. 4). Those units not crossed by the 56/12-1 well have been interpreted based on the correlation with the well 56/18-1 (Fig. 2), located 35 km towards the SE in the Fastnet Basin. The sea-level curve from Miller, K. G. et al. (2005) is displayed.

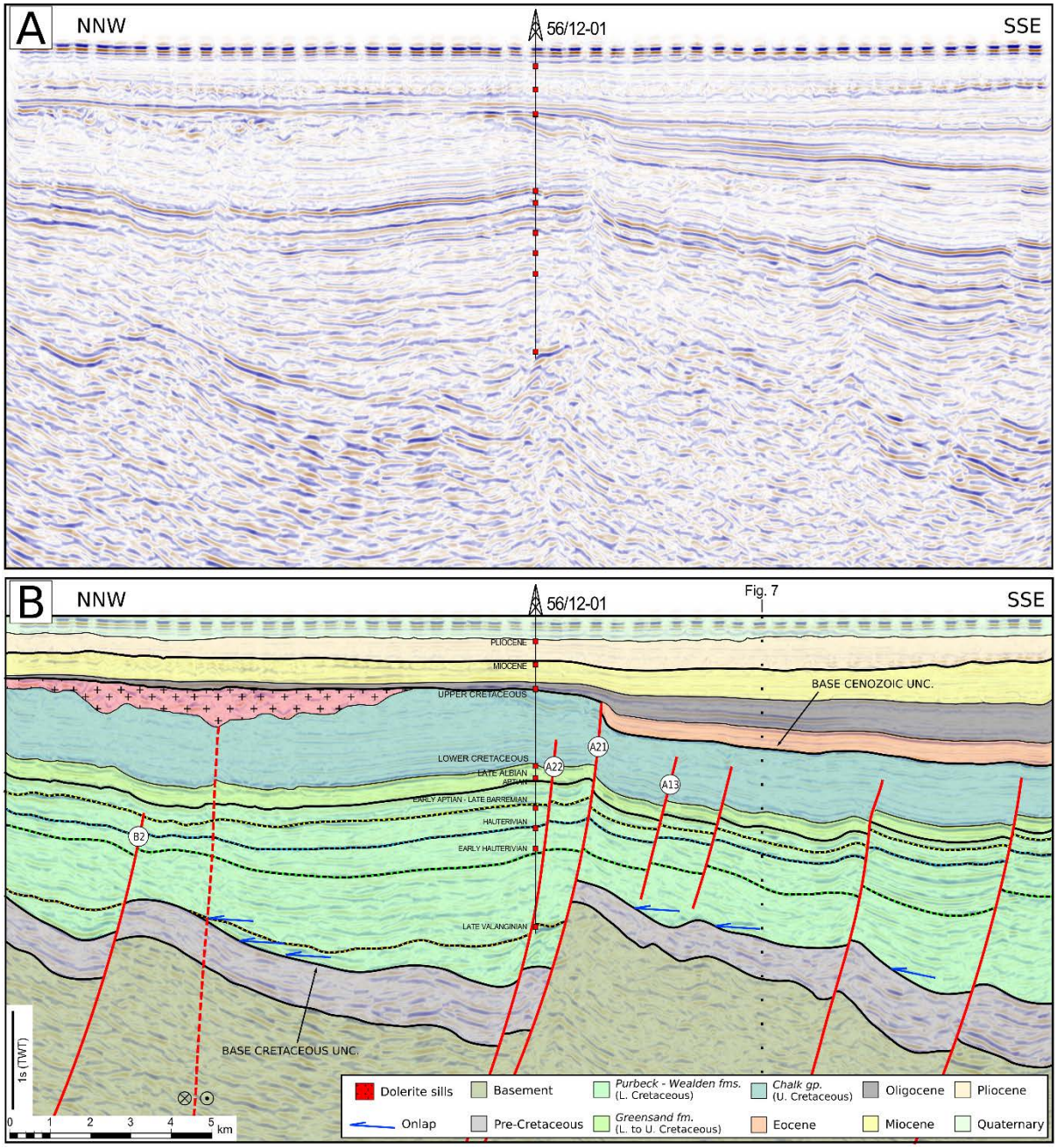

Figure 4. Arbitrary (a) seismic line and (b) interpreted seismic line along a NNW - SSE orientation. This line is perpendicular to the NE-SW-striking basin bounding faults and intersects the only well drilled in the Mizen basin (well 56/12-1). The line location is shown in Fig. 2.

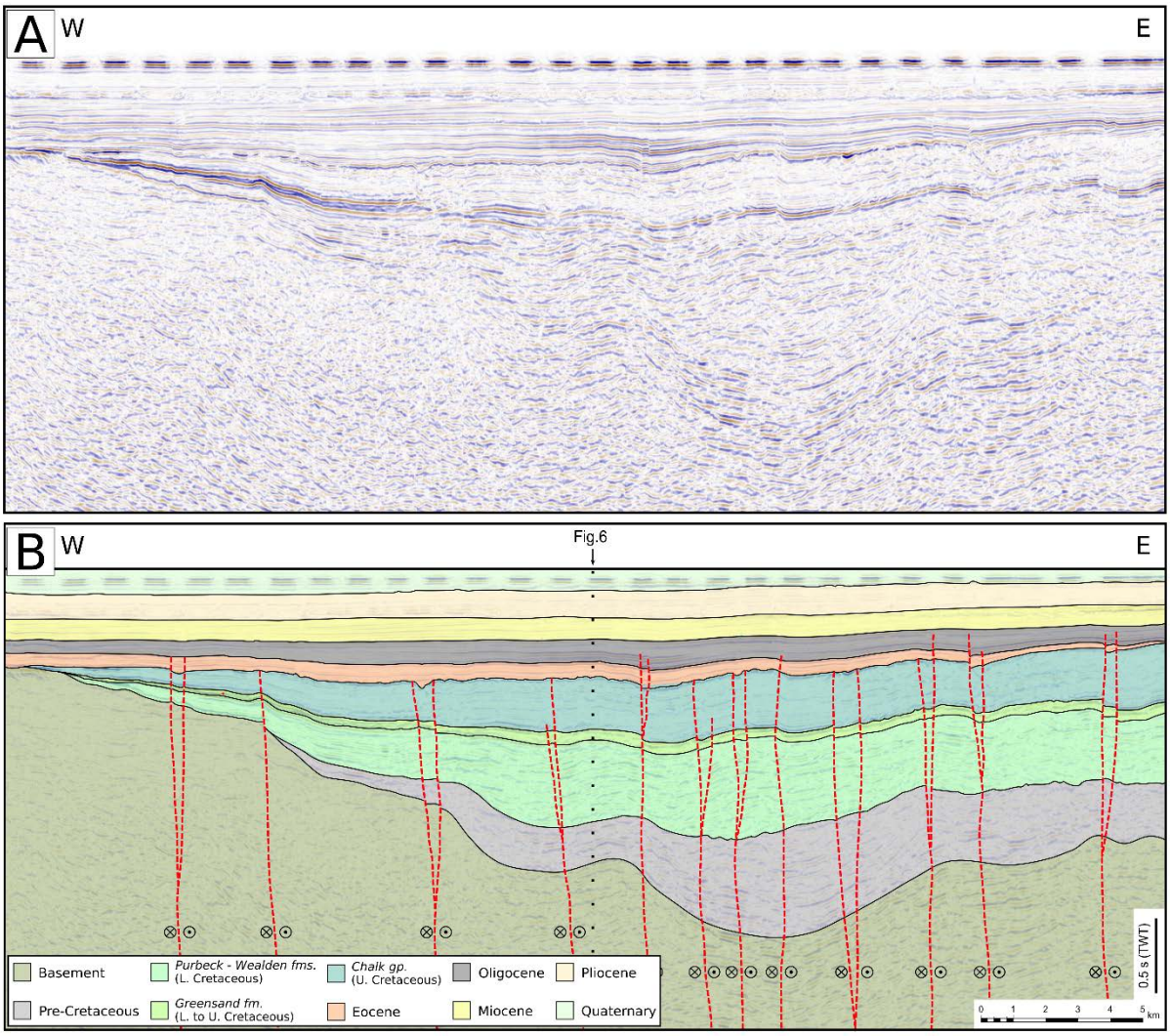

Figure 5. Arbitrary (a) seismic line and (b) interpreted seismic line in an E-W orientation along the footwall of the fault system A. This line is perpendicular to the NW-SE-striking strike slip faults and shows the Fastnet Spur in the W. The line location is shown in Fig. 2.

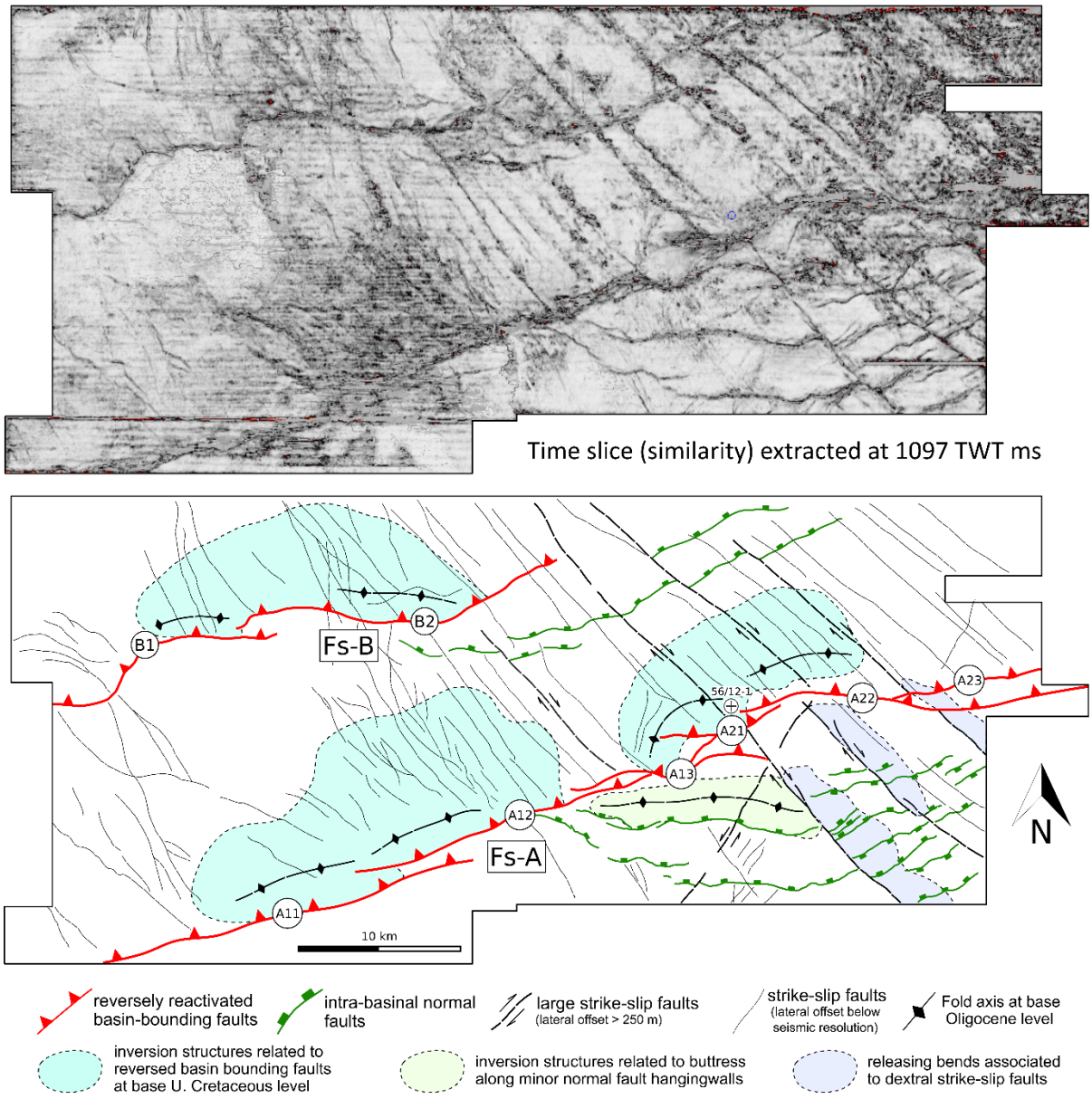

Figure 6. Uninterpreted (above) and interpreted (below) timeslice of the seismic variance attribute showing the main structural elements identified within the area covered by 3D seismic data. The map location is shown in Figs 1 and 2.

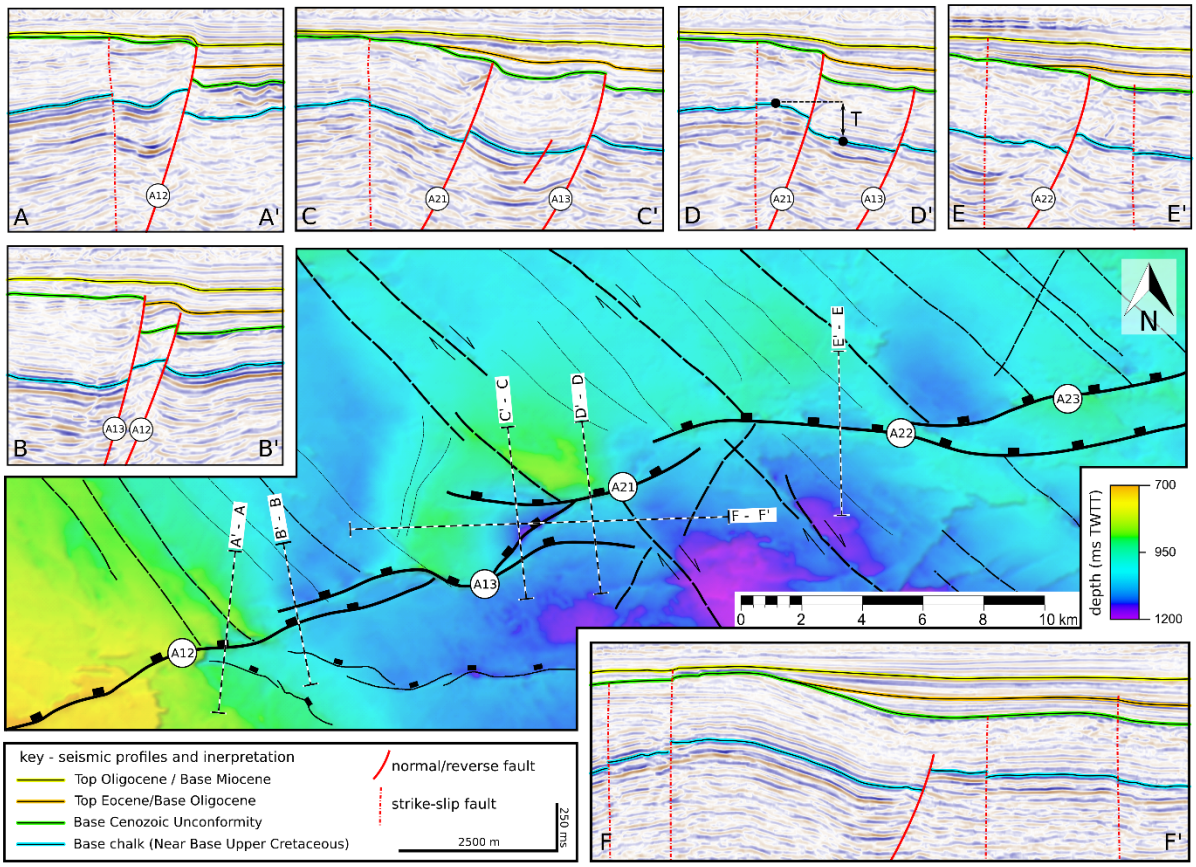

Figure 7. Structure contour map of the base Upper Cretaceous horizon and detailed views of selected arbitrary seismic lines along the main fault segments defining the fault system A.

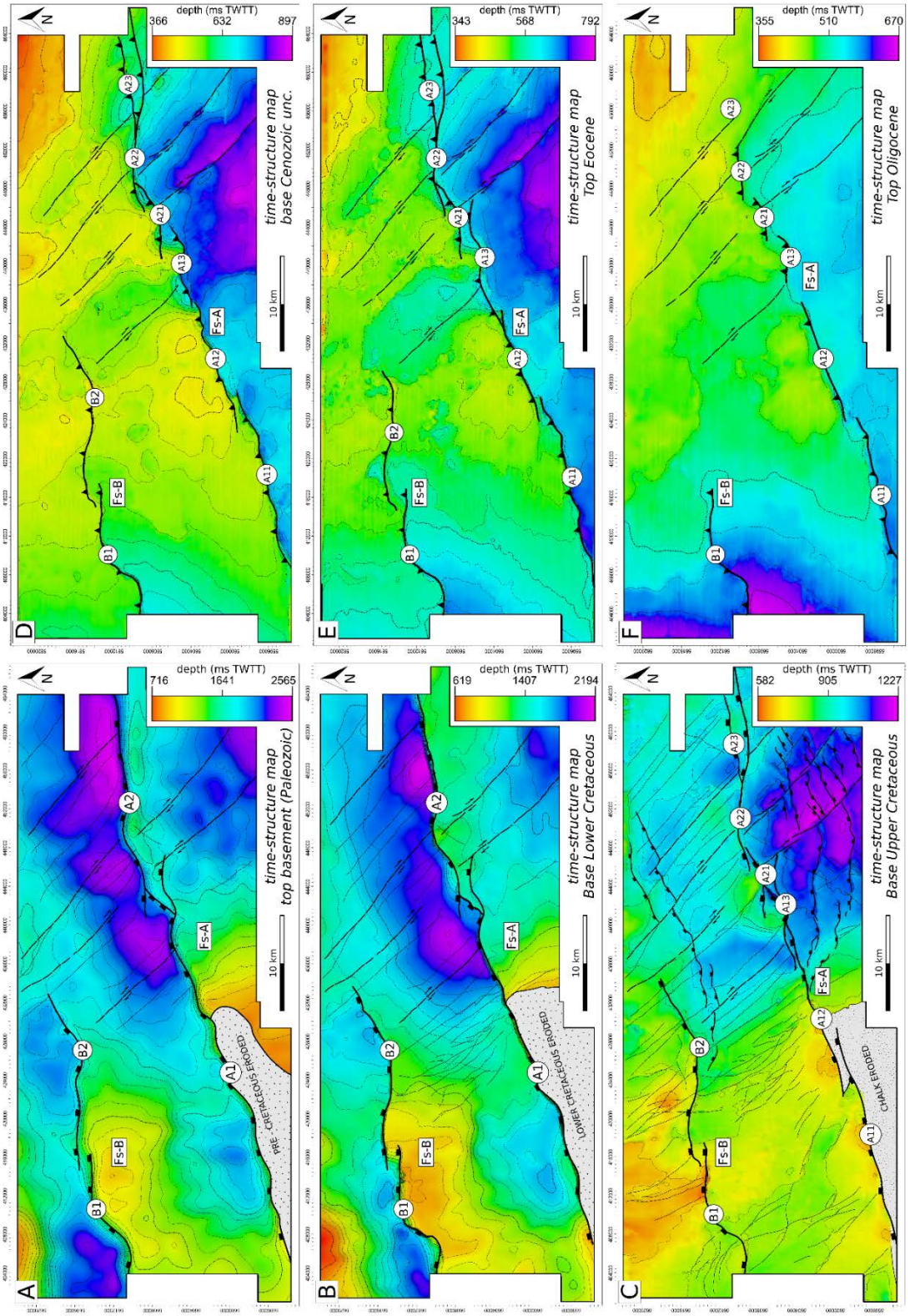

Figure 8. Time-structure maps illustrating the structural style of three rift-related (a-c) and three inversion-related (d-f) key horizons. The main structural elements observed in these maps are summarised in Fig. 8. For location see Figs 1 and 2.

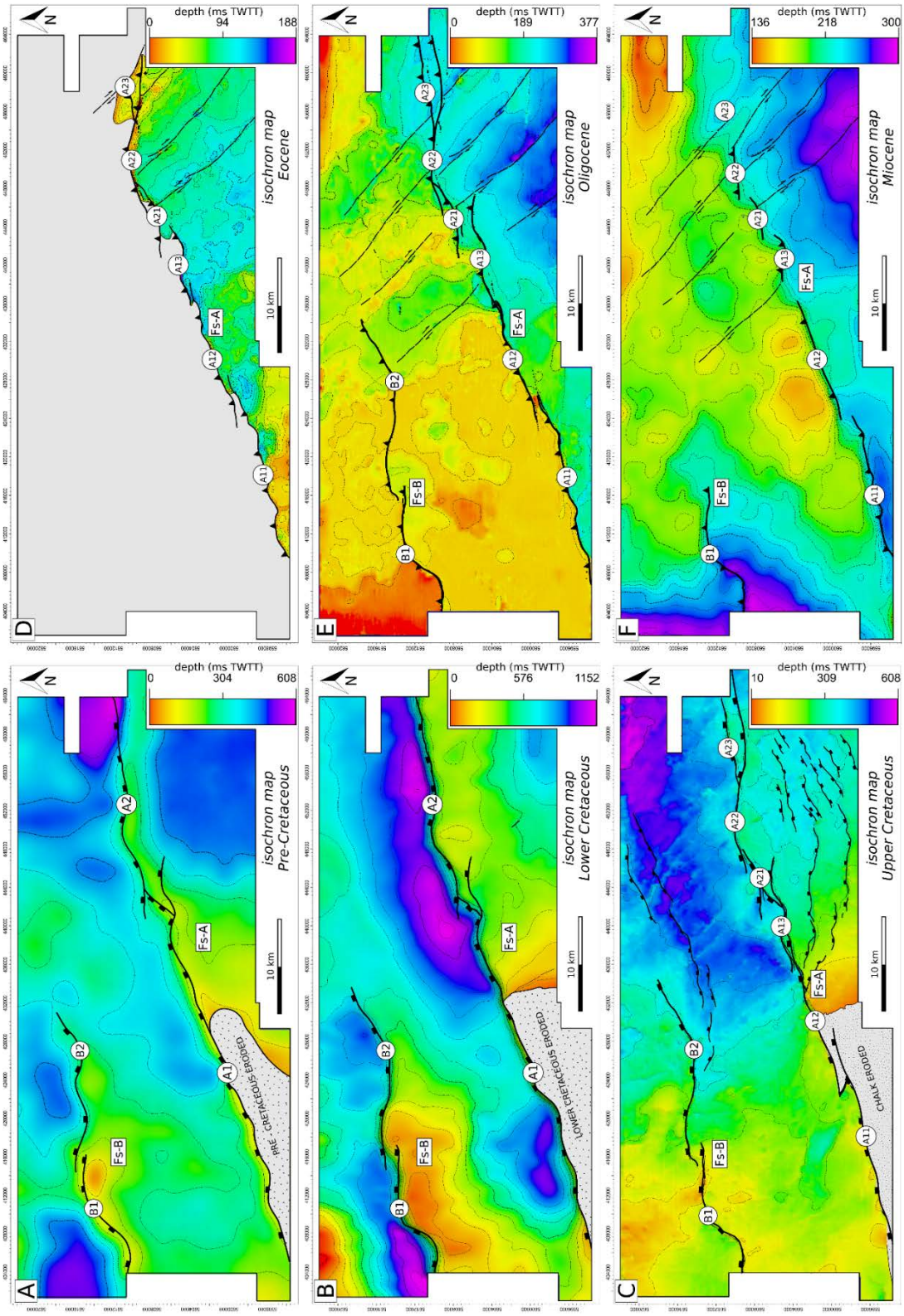

Figure 9. Isochron (vertical thickness) maps illustrating the evolution of the different tectonic phases and depocentre distribution. The maps a, b and c correspond to syn-rift and pre-inversion related units, the maps d, e and f correspond to syn-inversion related units. For location see figs. 1 and 3.

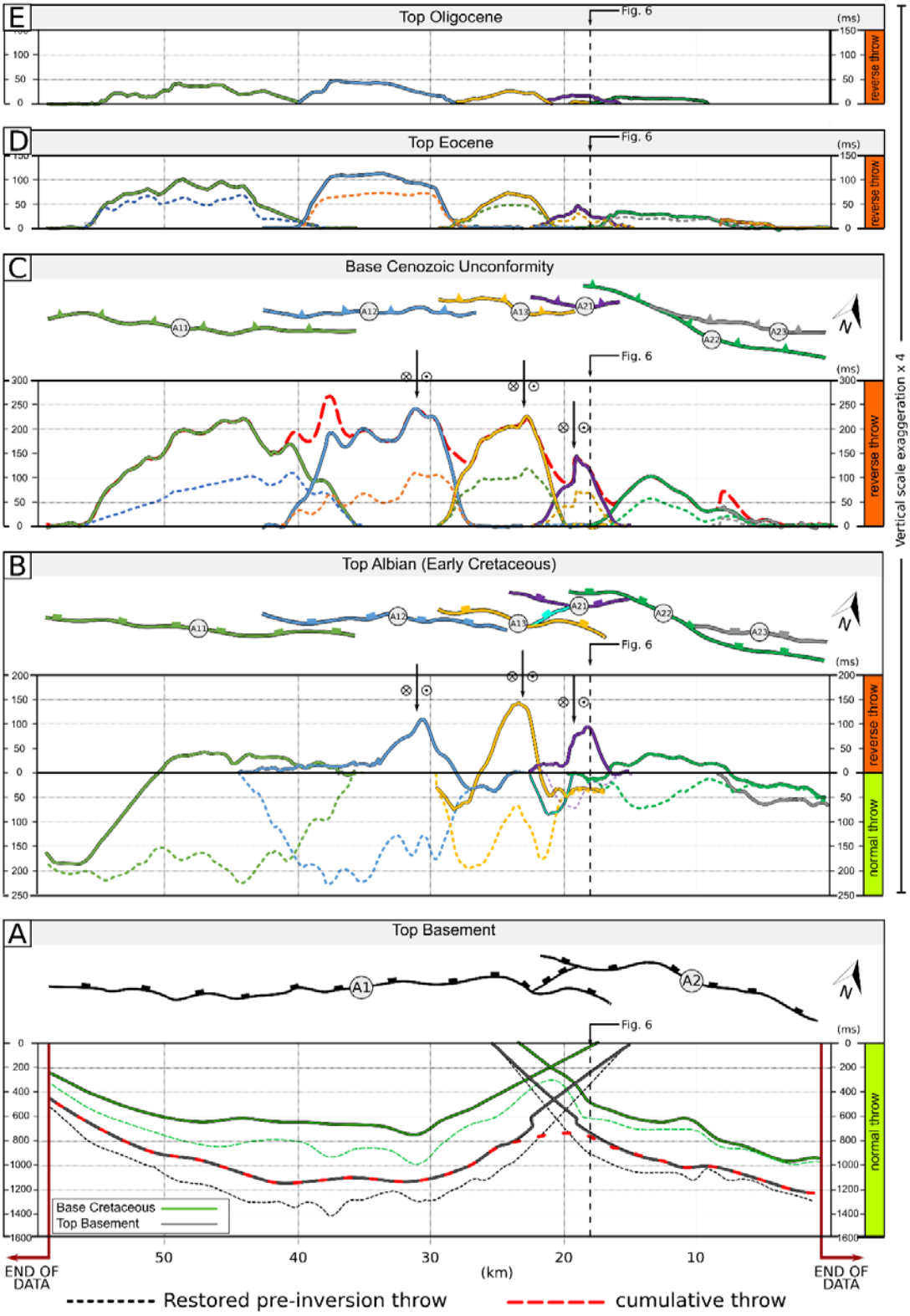

Figure 10. Throw vs. along strike distance plots for the fault system A for syn-rift and pre-inversion (a and b) and syn-inversion (c, d and e) key horizon. Dashed lines in (a) and (b) are profiles of normal throw obtained by subtracting the inversion values recorded on the profiles in (c). Fault throws were sampled every 10 m along the fault. Dashed lines in (d) and (c) are throw profiles obtained by subtracting the throw on the overlying horizon.

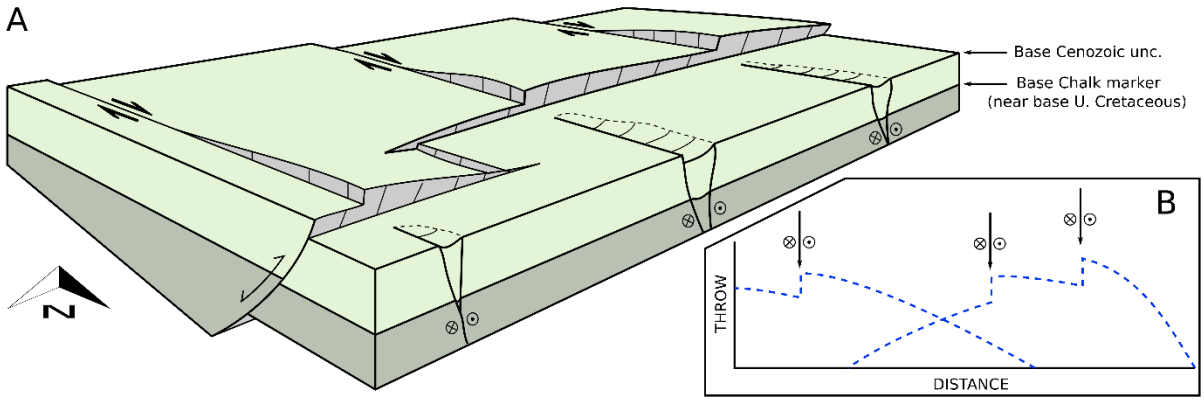

Figure 113. Schematic diagram showing the relationship between the main basin bounding fault system A (FS-A) and the larger strike-slip faults and an illustrative throw profile of the inverted normal fault.

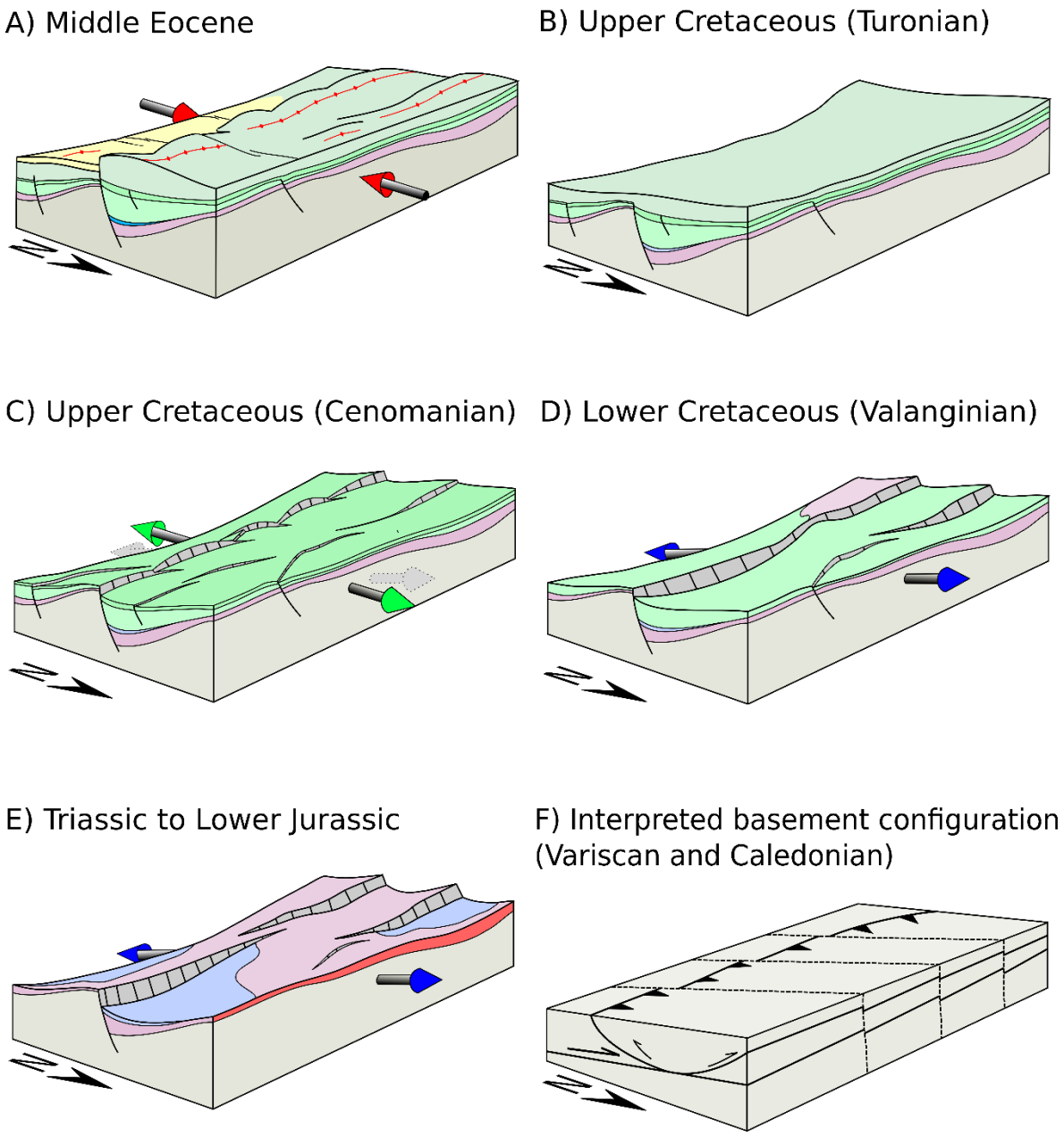

Figure 14. Schematic block diagrams showing the evolution of the Mizen Basin (see text).